Ricerca di Sistema elettrico

Experimental tests on the HLM facility NACIE-UP

M. Angelucci, R. Marinari

EXPERIMENTAL TESTS ON THE HLM FACILITY NACIE-UP

M. Angelucci, R. Marinari (ENEA)

Settembre 2015

Titolo

Experimental tests on the HLM facility NACIE-UP

Descrittori

Tipologia del documento:

Collocazione contrattuale: Accordo di programma ENEA-MSE su sicurezza nucleare e reattori di IV generazione

Argomenti trattati: Generation IV reactors

Tecnologia dei metalli liquidi

Sommario

The NACIE-UP experimental facility at the ENEA Brasimone Research Centre (Italy) allowed to evaluate the heat transfer coefficient of a wire-spaced fuel bundle cooled by lead-bismuth eutectic (LBE). Lead or lead-bismuth eutectic are very attractive as coolants for the GEN-IV fast reactors due to the good thermo-physical properties and the capability to fulfil the GEN-IV goals. Nevertheless, few experimental data on heat transfer with heavy liquid metals (HLM) are available in literature. Furthermore, just a few data can be identified on the specific topic of wire-spaced fuel bundle cooled by HLM. Additional analysis on thermo-fluid dynamic behaviour of the HLM inside the sub-channels of a rod bundle is necessary to support the design and safety assessment of GEN. IV/ADS reactors.

In this context, a wire-spaced 19-pin fuel bundle was installed inside the NACIE-UP facility. The pin bundle is equipped with 67 thermocouples to monitor temperatures and analyse the heat transfer behaviour in different sub-channels and axial positions.

The experimental campaign was part of the SEARCH FP7 EU project to support the development of the MYRRHA irradiation facility (SCK-CEN). Natural and mixed circulation flow regimes were investigated, with sub-channel Reynolds number in the range $\mathrm{Re}_{sc} = 10^3 - 10^4$ and heat flux in the range $q'' = 50 - 500 \left[kW/m^2 \right]$.

Local Nusselt numbers were calculated for five sub-channels in different ranks at three axial positions. Section-averaged Nusselt numbers were also calculated with two different definitions. Local Nusselt data showed good consistency with some of the correlation existing in literature for heat transfer in liquid metals for rod bundles. Local Nusselt numbers in peripheral ranks are lower, due to the presence of the hexagonal external wrap which affects the temperature profile.

Note

Other authors: M. Angelucci, R. Marinari

Copia n.   **In carico a:**

REV.	DESCRIZIONE	DATA		NOME / FIRMA	REDAZIONE	CONVALIDA	APPROVAZIONE
2			NOME				
			FIRMA				
1			NOME				
			FIRMA				
0	EMISSIONE	19/09/2015	NOME	I.Di Piazza	M. Tarantino	M. Tarantino
			FIRMA			

LIST OF CONTENTS

- **INTRODUCTION**

In the frame of the research activities planned to support the development of the MYRRHA irradiation facility (SCK-CEN), ENEA assumed the commitment to run experimental tests to simulate the thermal-hydraulic behavior of a wire-spaced fuel pin bundle cooled by heavy liquid metal. These activities, which were performed in the context of the European FP7 SEARCH Project, will support the Front End Engineering Design of the MYRRHA irradiation facility.

The experimental campaign is implemented on the NACIE (NAtural CIrculation Experiment) loop, located at ENEA Brasimone Research Centre, which was instrumented and refurbished to achieve these goals. The Upgraded facility is in the NACIE-UP configuration.

NACIE-UP is a rectangular loop which allows to perform experimental campaigns in the field of the thermal-hydraulics, fluid-dynamics, chemistry control, corrosion protection and heat transfer and to obtain correlations essential for the design of nuclear plant cooled by heavy liquid metals. The primary circuit basically consists of two vertical pipes (O.D. 2.5"), working as riser and downcomer, connected by two horizontal pipes (O.D. 2.5"). Then, the facility consists of an ancillary gas system (for the cover gas and the injection systems) and a pressurized water (16 bar) secondary side for heat removal. Moreover a fill and drain system is installed to allow the right operation of the loop. A full description of the NACIE-UP facility is reported in Section ⊡.

The test section for the experiments about the thermal-hydraulic behavior of a wire-spaced fuel pin bundle consists of 19 electrical pins with an active length $L_{active} = 600$ *mm.* The pin have a diameter $D = 6.55$ *mm*, and the maximum wall heat flux will be close to 1 *MW/m²*. The pins are placed on an hexagonal lattice by a suitable wrapper, while spacer grids will be avoided thanks to the wire spacer. This fuel pin bundle configuration is relevant for the MYRRHA's core thermal-hydraulic design [1].

The experiment was designed in order to analyze the thermal-hydraulic behavior of the MYRRHA FA during a Loss of Flow Accident (LOFA) with the coast-down of the main circulation pump. Heat transfer during a LOFA is driven by the inertia of the fluid during the pump coast-down and the onset of natural circulation due to the difference in height between the heat source and the heat sink. As a consequence of a LOFA, a stationary natural circulation flow rate will be established in a characteristic time which depends on the specific geometry of the system under consideration and on the geometry of the bundle.

Actually, some differences exist between the MYRRHA bundle and the NACIE-UP bundle. One is the number of ranks and pins: 7 ranks and 127 pins for MYRRHA against 3 ranks and 19 pins for NACIE-UP. This difference in the number of pins is not relevant for the convective heat transfer in the subchannels because side, corner and central subchannels can be monitored in the 19 pin bundle and basic phenomenology is the same as in the MYRRHA bundle. For a fixed average velocity in the bundle, pressure drops are expected to be a little higher in the NACIE-UP bundle because the influence of the wall is stronger, but from the literature and from numerical evidences [2], it is clear that this difference is not really relevant. The subchannel velocity u_{sc} determines, on the base of the geometry of the bundle and on the fluid properties, the LBE mass flow rate in the MYRRHA FA $\dot{m}_{FA}$ [kg / s], and the LBE mass flow rate in the NACIE-UP bundle $\dot{m}_{NACIE}$ [kg / s]. On the other

side, the linear power density Q_{lin} [kW/m] fixes the total power of the NACIE-UP 19-pin bundle $Q[kW]$.

Actually, the NACIE-UP facility can reach mass flow rates up to ~6 kg/s and both the bundle and the Heat Exchanger are designed for a maximum power of ~250 kW. In practice, this theoretical range is limited by the maximum clad temperature to safely operate the electrical pin T_{clad} < 550 °C. All these considerations were taken into account into defining the experimental test matrix, described in Section ⬜.

In this document, the post-test analyses for the experimental tests are described. A complete description of the post processing methods is reported in Section ⬜. The treatment of acquired data and the computation of derived quantities is fully explained. The error treatment method, which is in accordance with the error propagation theory, is also described.

Section ⬜ shows the main results on heat transfer obtained from the experimental tests performed at ENEA Brasimone Research Centre with the mock-up of the MYRRHA FA placed in the NACIE-UP facility. Different methods for the evaluation of both local and section-averaged heat transfer coefficients are presented. These methods are discussed and the results compared with the correlations existing in literature. Then, the main results on the coolability of the MYRRHA fuel assembly are summarized in Section 5.

Finally, the main conclusion are illustrated in Section 6.

- ## THE UPGRADE OF THE NACIE FACILITY (NACIE-UP): AN OVERVIEW

NACIE-UP is a rectangular loop which allows to perform experimental campaigns in the field of the thermal-hydraulics, fluid-dynamics, chemistry control, corrosion protection and heat transfer and to obtain correlations essential for the design of nuclear plant cooled by heavy liquid metals. It basically consists of two vertical pipes (O.D. 2.5"), working as riser and downcomer, connected by two horizontal pipes (O.D. 2.5"). In the NACIE-UP configuration, the whole height of the facility is about 8 meters, while the horizontal length is about 2,4 *m*. In the bottom of the riser a prototypical wire-spaced fuel pin bundle simulator (FPS), with a maximum power of 235 kW, have been installed. A proper heat exchanger is placed in the upper part of the downcomer.

NACIE-UP is made in stainless steel (AISI 304) and can use both lead and the eutectic alloy LBE as working fluid (about 2000 *kg*, 200 *l* in the updated configuration). It was designed to work up to 550°C and 10 bar. The difference in height between the center of the heating section and the center of the heat exchanger is about 5.5 m, and it is very important for the intensity of the natural circulation. In the riser, an argon gas injection device ensures a driving force to sustain forced convection in the loop.

The reference for the piping and instrumentation is the P&ID reported in Figure 1, where all the instrumentation, components and pipes are listed and logically represented. A schematic layout of the primary circuit is reported in Figure 2.

The facility includes:

- The Primary side, filled with LBE, with 2 ½" pipes. It consists of two vertical pipes , working as riser and downcomer, two horizontal pipes and an expansion tank;

- A new Fuel Pin Simulator (19-pins) 250 *kW* maximum power, placed in the bottom of the riser of the primary side;

- A Shell and tube HX with two sections, operating at low power (5-50 *kW*) and high power (50-250 *kW*). It is placed in the higher part of the downcomer;

- A high mass flow rate induction flow meter (3-15 *kg/s*) FM102, located in the downcomer, after the HX;

- 5 bubble tubes to measure the pressure drops across the main components and the pipes;

- Several bulk thermocouples to monitor the temperature along the flow path in the loop;

- The Secondary side, filled with water at 16 *bar*, connected to the HX, shell side. It includes a pump, a pre-heater, an air-cooler, by-pass and isolation valves, and a pressurizer (S201) with cover gas;

- An ancillary gas system, to ensure a proper cover gas in the expansion tank, and to provide gas-lift enhanced circulation;

- A LBE draining section, with ½" pipes, isolation valves and a storage tank (S300);

The ancillary gas system is practically identical to the previous configuration of the NACIE facility and does not have significant upgrade. It has the function to ensure the cover gas in S101 and to manage the gas-lift system in the riser (T103) for enhanced circulation regime.

The primary system is ordinary filled with liquid LBE and it is made by several components, pipes and coupling flanges. Pipes T101, T102, T103, T104, T105 are austenitic SS AISI304 2.5"S40, I.D. 62.68 *mm*. Figure 3 shows a picture of the primary side of the NACIE-UP facility.

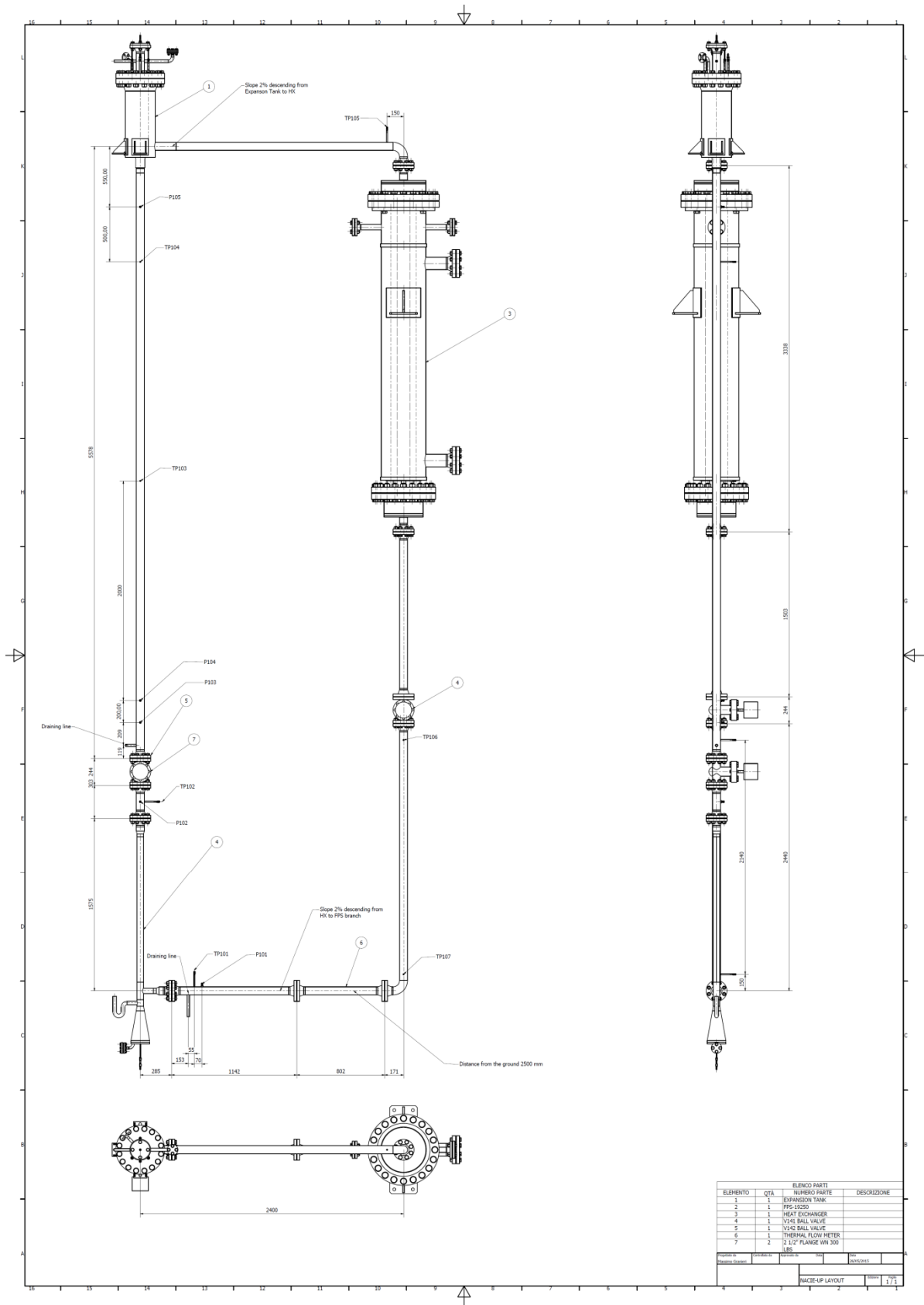*Figure.1: Piping and Instrumentation Diagram (P&ID) of the NACIE-UP facility.*

Figure.2: Schematic layout of the NACIE-UP facility.

Figure.3: NACIE-UP facility.

The main component of the primary loop is the instrumented Fuel Pin Bundle Simulator (FPS-19250), and it is fully described in Sections ?o and ?o. Most of the hydraulic resistance of the loop is in the wire-spaced FPS and thus it is very important to correctly measure the pressure drop across it through the F501 and F502 bubble tubes. The isolation 2.5" ball valve V142, placed downstream the FPS, will protect the FPS during the draining of the facility and will be partially closed to regulate the mass flow rate through the loop.

An expansion tank (S101) is located at the end of the riser and is partially filled with Argon as cover gas to control the pressure inside the primary circuit. Two level sensors LD101, LD102, are located respectively 80 and 180 *mm* above the outlet nozzle of the riser, inside the expansion vessel.

A drawing of the expansion vessel (S101) is reported in Figure.*4*. Pipe 1 in Figure.*4* is welded to the pipe working as riser (T103) and ends with a nozzle 285 *mm* long inside the tank.
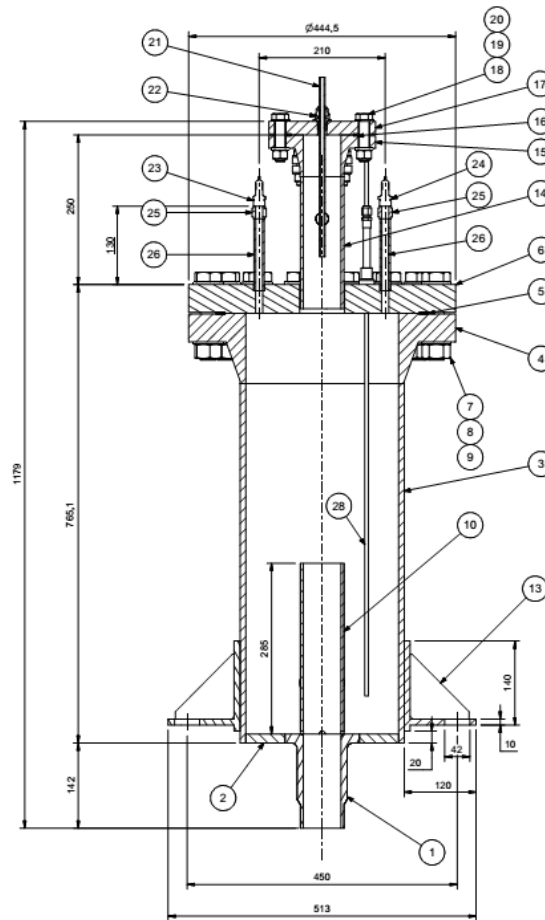
Figure.4: Layout of the expansion vessel inside the primary circuit of the NACIE-UP facility.

The fill and drain system has been designed to be completely controlled by DACS, and the fill and drain operational procedures are fully described in [3]. This system is made of austenitic SS AISI304 1/2" pipes, isolation valves, a filter (T305) and a storage tank (S300). In Figure.*5* some components of the fill and drain system are shown.

Figure.5: Sketches of the fill and drain system of the NACIE-UP facility.

In the riser, an argon gas injection device ensures a driving force to sustain enhanced circulation regime in the loop. The gas injection system is composed of a 9 *mm* I.D. pipe inserted inside the riser and is connected to the ancillary gas system. The pipe is 6135 mm long starting from the 2 ½" coupling flange in the upper part expansion tank and ends with a 4.35 *mm* I.D. hook-shaped pipe. More details on the operation of the gas injection system are described in [4].

The flow meter FM102 is based on the magnetic induction effect and is accurate for relatively 'high' mass flow rates (5-20 kg/s). FM102 has been tested in the last configuration of NACIE in December 2012 and results are documented in [5].

The secondary side is a 16 *bar* pressurized water loop, with a circulation pump PC201, a pre-heater H201, the HX shell side, an air-cooler E201 and a pressurizer S201. Components of the secondary side are depicted in Figure.*6*. The pressurizer is connected to the gas lines to ensure an Argon cover gas and to regulate the loop pressure though DACS. Most of the valves are motorized in order to ensure the full operability of the secondary loop by DACS. The valve system allows to drain and fill the two sections of the HX shell separately from the control room. A bypass of the HX is ensured by V214 for the pre-heating of the secondary water. The heating section H201 allows to heat-up the

secondary fluid to have flexibility in managing low FPS powers. The ultrasonic flow meter FM201 allows to monitor the secondary water mass flow rate, while several thermocouples will monitor temperature in the loop; the combination of the two information will allow to quantify the power exchange in the HX. The heat exchanger is shell and tube type and has been designed to exchange heat up to 250 *kW*. Two separated shell sections have been built: a counter-current high-power section (0-30 *kW*) and a cross-flow low power section (30-250 *kW*), both connected to the pressurized water secondary side. The two sections can be drained and filled separately. More details about the Shell and tube HX are provided in [6], while the operational process and procedures are of the secondary side are documented in [3].

Figure.6: Components of the secondary side of the NACIE-UP facility.

o **The fuel pin bundle simulator**

The FPS will consist of 19 electrical pins with an active length L_{active} = 600 *mm.* The whole length (L_{total} = 2000 *mm)* includes the *non-active* length and the electrical connectors. The pin have a diameter *D*=6.55 *mm*, and the maximum wall heat flux will be close to 1 *MW/m²*. The pins will be placed on an hexagonal lattice by a suitable wrapper, while spacer grids will be avoided thanks to the wire spacer. The maximum power of the new fuel pin bundle is ~ 235 kW. To simulate the fuel pins, an electrically heated rod bundle has been specifically designed and provided by THERMOCOAX for this purpose. This fuel pin bundle configuration is relevant for the MYRRHA's core thermal-hydraulic design [1].

Some dimensions of the fuel bundle and an overall sketch of the cross section are reported in Figure.*8*.
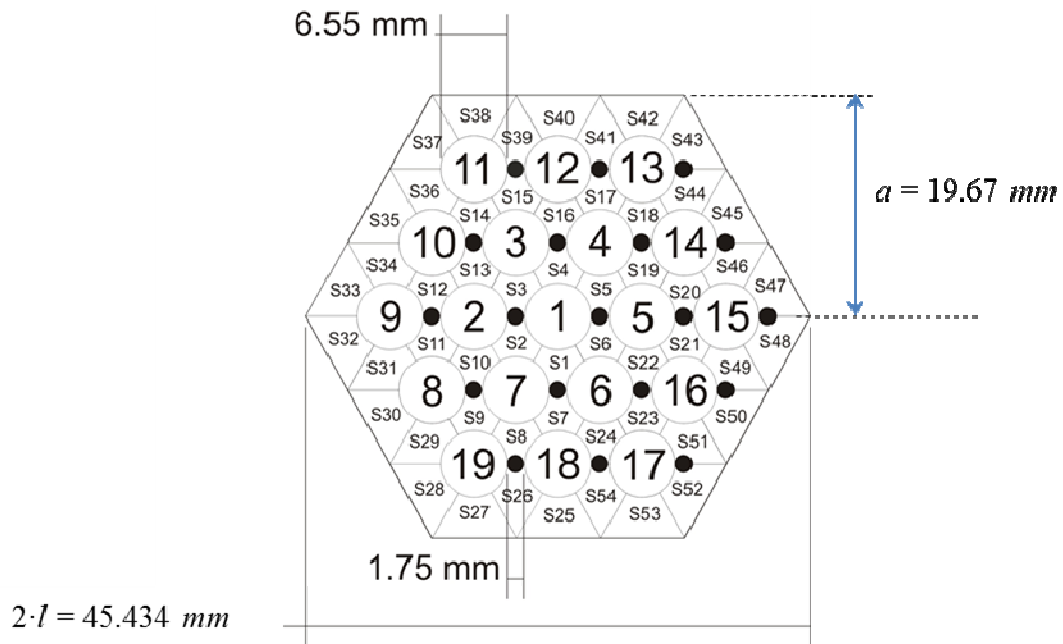

Figure 7: Cross-section of the electrical wire-spaced fuel pin bundle simulator to be used at ENEA.

The main geometrical dimensions to be considered for a thermal-hydraulic assessment of the FA are:

- The rod diameter *D*=6.55 *mm*;

- The wire diameter *d*=1.75 *mm*;

- The pitch to diameter ratio *P/D*=(*D*+*d*+δ)/*D*=1.2824, which keeps into account the nominal gap between the wire and the neighbor pins δ=0.1 *mm*;

- The distance between the last rank of pins and the internal wall of the wrap δ_w=*d*+δ =1.75+0.1 *mm*= 1.85 *mm*;

- Wires are helicoidally twisted around each pin with a streamwise pitch of P_w=262 *mm*;

- The regular lattice is triangular/hexagonal staggered.

The total flow area can be conventionally divided into 54 subchannels of different ranks (S1-S54). Pins and subchannels have been numbered to better define the instrumentation needed as well as the physical phenomena involved. The subchannels and the relative pins that will be instrumented are also indicated in Figure.*8*. Details about the fuel pin bundle instrumentation are described in Section ▯o.
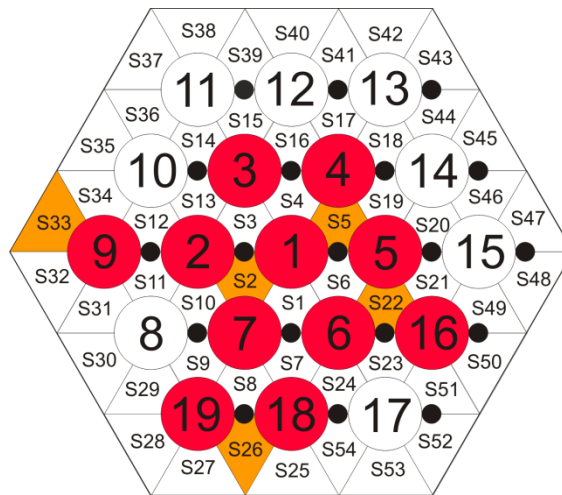
- *Figure.8: Sketch fuel pin bundle simulator for the NACIE facility.*
  Instrumented pins in red; instrumented subchannels in orange, wire in black.

The internal dimension of the wrap can be computed by keeping into account that the apothem *a* of the internal walls of the hexagonal wrapper.

$$a = 2P\frac{\sqrt{3}}{2} + \frac{D}{2} + d + \delta = 19.674 \ mm \qquad (1)$$

The side length *l* is simply $l = 2a/\sqrt{3} = 22.7178 mm$. In such a way the dimensions of the wrap are fixed according to what required by the MYRRHA FA design.

The geometry shown in Figure *7* allows to study and characterize heat transfer and fluid flow during a LOFA for three different ranks of rods in the MYRRHA FA:

- the external rank *N*, represented by the pins 8-19 and by subchannels S25-S54;

- the rank *N*-1, represented by pins 2-7 and by subchannels S7-S24;

- the central rank, represented by the central pin n. 1 and by subchannels S1-S6;

These three ranks are representative of all the subchannels in the MYRRHA FA. In fact, it is well known from the literature that for wire-wrapped bundles of similar geometry, the influence of the wall is considered important for the external rank *N* and for the *N*-1 rank of pins, while the other ranks are not so much influenced by the wrap wall. Moreover, in principle, the 19-pins bundle will allow to distinguish between the corner pins like 9 or 11 and the pure *N* rank pins like 10 or 12.

The equivalent diameter of such configuration can be easily computed, by keeping into account that the cross-sectional area of the hexagonal wrap is $A_{wrap} = 3l^2\sqrt{3}/2$, while the total area of the pins and the wire is respectively $A_{pins} = M\pi D^2/4$, $A_{wire} = M\pi d^2/4$, with *M*=19 is the number of

the pins. The wetted perimeter is $L_w = M(\pi D + \pi d) + 6l$. The resulting equivalent diameter can be computed as:

$$D_{eq} = \frac{4(A_{wrap} - A_{pins} - A_{wire})}{L_w} = 4.147\ mm \tag{2}$$

which is slightly higher than the nominal equivalent diameter $D_{eq,nom} \approx 3.86\ mm$ of an infinite lattice with the same geometrical features. However, the influence of the wall on this parameter is quite small for a 19-pins bundle. The nominal equivalent diameter will be used to define the non-dimensional quantities in the post-processing of the results, as agreed with SCK [7].

Several dimensionless groups can be defined on the facility to characterize the thermal-hydraulic phenomena involved. Calling by u the average velocity in the 2.5" tube of diameter d_t and section A, a tube Reynolds number can be defined as:

$$Re_{tube} = \frac{u\,d_t}{\nu} \tag{3}$$

This number gives a first reference for the convective heat transfer. The velocity u, and thus the overall mass flow rate $\dot{m} = \rho u A$ can be generated both by natural circulation, i.e. by buoyancy forces, and by forced circulation, i.e. by some source of momentum like a pump or the gas-lift injection system.

The role of the natural circulation is expressed by the Grashof number:

$$Gr = \frac{g\,\beta\Delta T H^3}{\nu^2} = \frac{v_{bv}^2 H^2}{2\nu^2} \tag{4}$$

The typical Brunt-Vaisala velocity of the gravity waves can be recognized as $v_{bv} = \sqrt{2g\,\beta\Delta T H}$ and represents the velocity of a grave in the modified buoyancy gravity field $g\beta\Delta T$.

The streamwise subchannel velocity u_{sc} in the bundle subchannel, can be computed considering that the mass flow rate is constant in all the sections of the loop, and thus:

$$u_{sc} = \frac{A}{A_{wrap} - A_{pins} - A_{wire}} \cdot u = \frac{3085.567}{654.965} \cdot u = 4.711 \cdot u \tag{5}$$

The subchannel Reynolds number can therefore be computed as:

$$Re_{sc} = \frac{u_{sc} D_{eq}}{\nu} = \frac{4.711 \cdot D_{eq}}{dt} \frac{u \cdot d_t}{\nu} = 0.290 \cdot Re_{tube} \tag{6}$$

The subchannel Reynolds number Re_{sc} is about 1/3 of the pipe Reynolds number Re_{tube} in NACIE-UP loop.

Pressure losses in the NACIE facility can be estimated via literature known correlations. Losses in the pin bundle appears the most important ones. Referring the global resistance coefficient K to the velocity u in the NACIE 2.5" pipe, it is possible to write K by the formula:

$$K = K_{tubes} + K_{conc} + K_{bundle} \tag{7}$$

where K_{tubes} refers to the losses in the loop pipes (horizontal and vertical branches), K_{conc} refers to the concentrated losses (i.e. elbows, expansion vessel and heat exchanger), K_{bundle} refers to the bundle losses. Details about formulas used to calculate the pressure losses in the fuel pin simulator bundle and in the whole NACIE-UP loop are mentioned in [6].

The overall layout of the fuel pin bundle simulator is depicted in Figure.*9*. It consists of the hexagonal wrap and additional parts and flanges to connect the bundle to the NACIE facility. The design pressure is 10 bar and the design temperature is 550°*C*. The lower non-active region of the bundle is more than 500 *mm* for thermal hydraulic reasons. A fully developed flow is required into the active zone inlet section for a proper run of the experiment. On the pin foot, a bottom grid is positioned to keep the bundle tight. Referring to the overall bundle layout, the conical portion allows the elastic bending of the pins which should be needed to allow the proper installation of the electrical connectors. All details regarding the components of the fuel pin bundle simulator and the wire installation around the pins can be found in [6].The overall picture of the fuel pin bundle assembled, before the installation in the NACIE-UP facility, is shown in Figure.*10*.

Figure.9: Overall bundle layout: technical drawing.

Figure.10: Fuel pin bundle simulator assembled before installation.

    ○ **Bundle Instrumentation**

As already pointed out, *Figure.8* represents a section, viewed from the top, of the bundle with pins and subchannels that must be instrumented.

Prototypical pins were already manufactured by THERMOCOAX for ENEA with the specification mentioned above for the LOFA experiment on the coolability of MYRRHA FA.

Pins 2, 4, 6, 7, 9, 16, 18, 19 are equipped with wall embedded thermocouples on a generatrix parallel to the pin axis, as shown in Figure.*11*. Three different levels will be considered: z= 38, 300, 562 mm starting from the beginning of the active region of the pins (connector side). Conventionally, measurement sections at z=38, 300 and 562 mm will be called respectively section *A*, *B* and *C*. The reference section in Figure *7* is referred at the section *A*, z=38 mm, and the other measurement sections chosen *B*, *C* (i.e. z=300, 562 mm) are exactly in the same configuration, being the wire pitch P_w=262 mm= 300-38 mm= 562-300 mm. Therefore this choice allows to have three independent measurements of heat transfer referred to the same relative position of wire and pins and this feature drops off systematic errors.
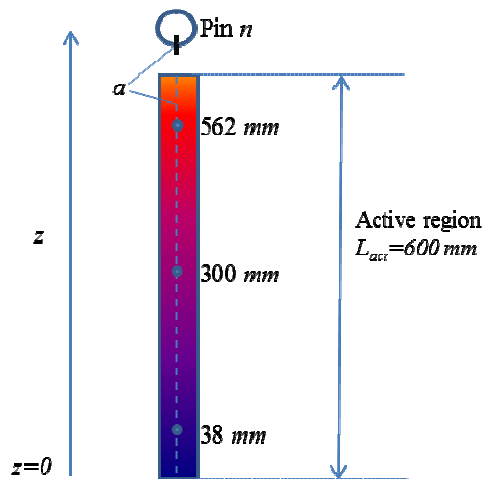

Figure.11: Wall Embedded TCs locations for pins n. 2,4,6,7,9,16,18,19.

Pin 1 is instrumented with wall embedded thermocouples on two generatrices *a* and *b*, located 180° each other, parallel to the pin axis, pin n. 5 will be instrumented along three generatices *a*, *c*, *d*, located at 120° each other, as it is shown in Figure 12.
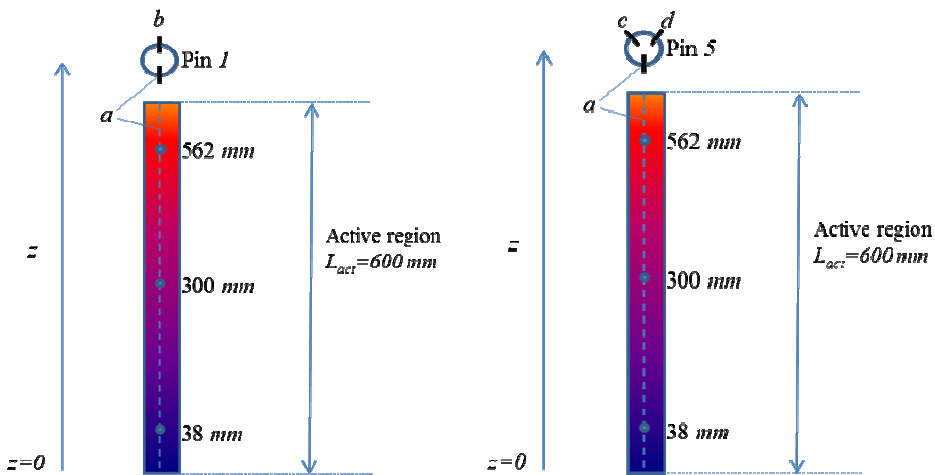
Figure.12: Wall Embedded TCs locations for pin n. 1 and n.5

Subchannels S2, S5, S22, S26, S33 are instrumented with bulk thermocouples 0.5 *mm* thickness at the 3 measurement sections A, B and C, i.e. at levels z=38, 300, 562 *mm*. The generic measurement section, with wall thermocouples and subchannels instrumented, is shown in a schematic view in Figure.*13*. The relative position of the grooves, i.e. of the generatrices (marked in **red**) for the different pins can be also deduced, considering the reference for the azimuthal pin angle ϑ, with positive angles anticlockwise *with the bundle section seen from the top*.

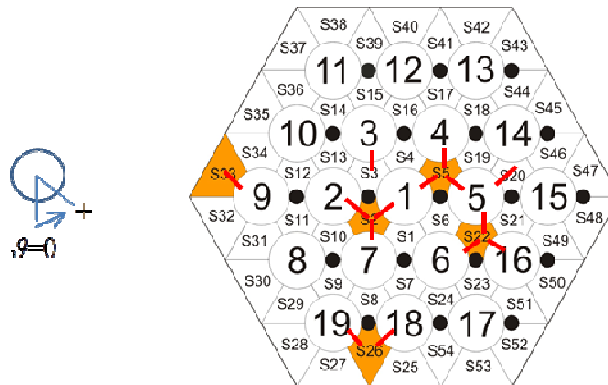*Figure.13: Generic measurement section (z=38, 300, 562 mm) conventionally view from the top, with the location of wall TCs and instrumented channels.*

The related azimuthal angles ϑ are reported in Table 1 for all measurement sections (z=38 *mm*, z=300 *mm*, and z=562 *mm*).

The bulk thermocouples run following the wire associated to the pin closest to the monitored subchannel. The association table between monitored subchannel and wire to be used to allocate bulk thermocouples with other relevant information is reported in Table 2 for the whole bundle.

Table.1: Azimuthal angles of the pin generatrices where the wall embedded Thermocouples are located.

Pin number	Azimuthal angles	Location [*mm*]	Number of	TC diameter

	ϑ[°]		wall TCs	[mm]
1	-60, +120	z= 38, 300, 562	6	0.35
2	+60	z= 38, 300, 562	3	0.35
3	0	z=38, 81.7, 125.3, 169, 212.7, 256.3,300, 343.7, 387.3, 431, 474.7, 518.3, 562	13	0.35
4	0	z= 38, 300, 562	3	0.35
5	-120,0,+120	z= 38, 300, 562	9	0.35
6	+120	z= 38, 300, 562	3	0.35
7	+180	z= 38, 300, 562	3	0.35
9	-120	z= 38, 300, 562	3	0.35
16	-120	z= 38, 300, 562	3	0.35
18	-60	z= 38, 300, 562	3	0.35
19	+60	z= 38, 300, 562	3	0.35

Table.2: Azimuthal angles of the generatrices where the bulk Thermocouples are located for each subchannel instrumented.

Subchannel number	Pin (wire) number	Azimuthal angle ϑ[°]	Location [mm]	Number of bulk TCs	TC diameter [mm]
S5	1	+120	z= 38, 300, 562	3	0.5
S2	2	+60	z= 38, 300, 562	3	0.5
S22	6	+120	z= 38, 300, 562	3	0.5
S33	9	-120	z= 38, 300, 562	3	0.5
S26	19	+60	z= 38, 300, 562	3	0.5

Pin number 3 is instrumented along a generatrix with 13 wall embedded thermocouples along the active length, placed every P_w/6=43.66 *mm* starting from *z*=38 *mm*; the azimuthal orientation of the groove is ϑ = 0.

The total number of wall embedded thermocouples is 52. Regarding the bulk thermocouples, they must be placed on 5 subchannels (S2, S5, S22, S26, S33) in 3 different sections (*A*, *B* and *C*, i.e. *z*=38, 300 and 562 mm) for a total number of bulk thermocouples of 15.

At each measurement section, wall embedded thermocouples must move azimuthally around the pin to reach the correct position/generatrix represented in Figure 13 and reported from Table 1 to Table *3*. On the other side, at each measurement section, bulk thermocouples must leave the wire and reach the center of the subchannel to monitor.

To increase the mechanical resistance of the bulk thermocouples placed into the LBE stream, and aiming to guarantee the correct position of them during the run of the experiment, the "prolonged" thermocouples type are adopted. That solution consist of to put the hot junction in the center of the monitored subchannel and to prolong the TC wire to form an arc (thus increasing its stiffness) and then to fix the TC head to the spacing wire by point welding.

Table **3** provides all the relevant information associated with the thermocouples, i.e. the Pin/wire number, the TC type ('Wall' or 'Bulk'), the TC diameter, the subchannel number for bulk TCs, the azimuthal angle, the vertical *z* location from the beginning of the active region and the corresponding measurement section 'A', 'B', or 'C'. In the cells where the information is not well defined the symbol '-' is used.

All the thermocouples adopted in the FPS are 'K' type pre-calibrated by the manufacturer (THERMOCOAX) with a certified accuracy of 0.1 K.

Table 3: Thermocouples names with all the relevant information associated.

TC name	Pin (wire) number	Type	TC diameter [*mm*]	Subchannel number (Bulk TC)	Azimuthal angle [°] (wall TC)	*z* Location [*mm*]	Section
TC-FPS-01	2	Bulk	0.5	S2	-60	38	*A*
TC-FPS-02	1	Bulk	0.5	S5	+120	38	*A*
TC-FPS-03	6	Bulk	0.5	S22	+120	38	*A*
TC-FPS-04	19	Bulk	0.5	S26	+60	38	*A*
TC-FPS-05	9	Bulk	0.5	S33	-120	38	*A*
TC-FPS-06	2	Bulk	0.5	S2	-60	300	*B*
TC-FPS-07	1	Bulk	0.5	S5	+120	300	*B*
TC-FPS-08	6	Bulk	0.5	S22	+120	300	*B*
TC-FPS-09	19	Bulk	0.5	S26	+60	300	*B*
TC-FPS-10	9	Bulk	0.5	S33	-120	300	*B*
TC-FPS-11	2	Bulk	0.5	S2	-60	562	*C*
TC-FPS-12	1	Bulk	0.5	S5	+120	562	*C*
TC-FPS-13	6	Bulk	0.5	S22	+120	562	*C*
TC-FPS-14	19	Bulk	0.5	S26	+60	562	*C*
TC-FPS-15	9	Bulk	0.5	S33	-120	562	*C*
TC-FPS-16	1	Wall	0.35	-	-60	38	*A*
TC-FPS-17	1	Wall	0.35	-	+120	38	*A*

TC-FPS-18	2	Wall	0.35	-	+60	38	A
TC-FPS-19	4	Wall	0.35	-	0	38	A
TC-FPS-20	5	Wall	0.35	-	-120	38	A
TC-FPS-21	5	Wall	0.35	-	0	38	A
TC-FPS-22	5	Wall	0.35	-	+120	38	A
TC-FPS-23	6	Wall	0.35	-	+120	38	A
TC-FPS-24	7	Wall	0.35	-	+180	38	A
TC-FPS-25	9	Wall	0.35	-	-120	38	A
TC-FPS-26	16	Wall	0.35	-	-120	38	A
TC-FPS-27	18	Wall	0.35	-	-60	38	A
TC-FPS-28	19	Wall	0.35	-	+60	38	A
TC-FPS-29	1	Wall	0.35	-	-60	300	B
TC-FPS-30	1	Wall	0.35	-	+120	300	B
TC-FPS-31	2	Wall	0.35	-	+60	300	B
TC-FPS-32	4	Wall	0.35	-	0	300	B
TC-FPS-33	5	Wall	0.35	-	-120	300	B
TC-FPS-34	5	Wall	0.35	-	0	300	B
TC-FPS-35	5	Wall	0.35	-	+120	300	B
TC-FPS-36	6	Wall	0.35	-	+120	300	B
TC-FPS-37	7	Wall	0.35	-	+180	300	B
TC-FPS-38	9	Wall	0.35	-	-120	300	B
TC-FPS-39	16	Wall	0.35	-	-120	300	B
TC-FPS-40	18	Wall	0.35	-	-60	300	B
TC-FPS-41	19	Wall	0.35	-	+60	300	B
TC-FPS-42	1	Wall	0.35	-	-60	562	C
TC-FPS-43	1	Wall	0.35	-	+120	562	C
TC-FPS-44	2	Wall	0.35	-	+60	562	C
TC-FPS-45	4	Wall	0.35	-	0	562	C
TC-FPS-46	5	Wall	0.35	-	-120	562	C

TC-FPS-47	5	Wall	0.35	-	0	562	*C*
TC-FPS-48	5	Wall	0.35	-	+120	562	*C*
TC-FPS-49	6	Wall	0.35	-	+120	562	*C*
TC-FPS-50	7	Wall	0.35	-	+180	562	*C*
TC-FPS-51	9	Wall	0.35	-	-120	562	*C*
TC-FPS-52	16	Wall	0.35	-	-120	562	*C*
TC-FPS-53	18	Wall	0.35	-	-60	562	*C*
TC-FPS-54	19	Wall	0.35	-	+60	562	*C*
TC-FPS-55	3	Wall	0.35	-	0	38	*A*
TC-FPS-56	3	Wall	0.35	-	0	81.7	-
TC-FPS-57	3	Wall	0.35	-	0	125.3	-
TC-FPS-58	3	Wall	0.35	-	0	169	-
TC-FPS-59	3	Wall	0.35	-	0	212.7	-
TC-FPS-60	3	Wall	0.35	-	0	256.3	-
TC-FPS-61	3	Wall	0.35	-	0	300	*B*
TC-FPS-62	3	Wall	0.35	-	0	343.7	-
TC-FPS-63	3	Wall	0.35	-	0	387.3	-
TC-FPS-64	3	Wall	0.35	-	0	431	-
TC-FPS-65	3	Wall	0.35	-	0	474.6	-
TC-FPS-66	3	Wall	0.35	-	0	518.3	-
TC-FPS-67	3	Wall	0.35	-	0	562	*C*

o **Data Acquisition and Control System (DACS)**

Data acquisition and instrumental control is fully achieved with the aim of LabVIEW System Design Software [8]. The primary and the secondary sides of the NACIE-UP facility can be remotely controlled. The operations of fill and drain of the plant can be made remotely as well. The ancillary gas system, instead, is directly controlled through the gas panel shown in Figure.*14*.
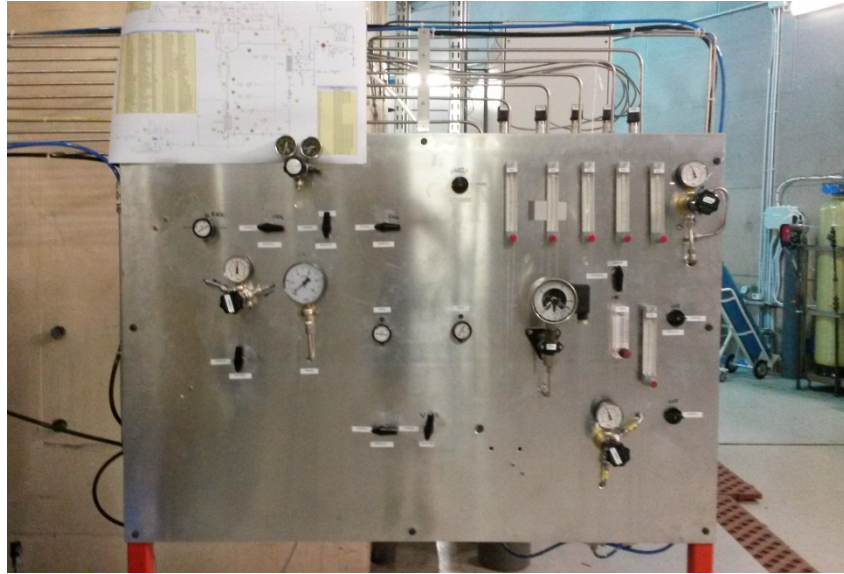

Figure.14: Manual panel for the gas system control

Figure 15shows the control and monitoring panel to remotely actuate components and valves. From this panel, temperatures and pressures inside the primary and secondary systems can be monitored. In Figure.*16* the remote control panel for the activation and the regulation of the power production can be seen. Power level ,number of pin activated and power ramp can be regulated as needed. Moreover, all the wall and bulk thermocouples inside the fuel pin bundle simulator can be constantly monitored from the panel displayed in Figure 17. Each pin can be controlled separately and this feature gives the opportunity to perform asymmetric heating tests for code validation. Ramps from a power level to another one are also possible.
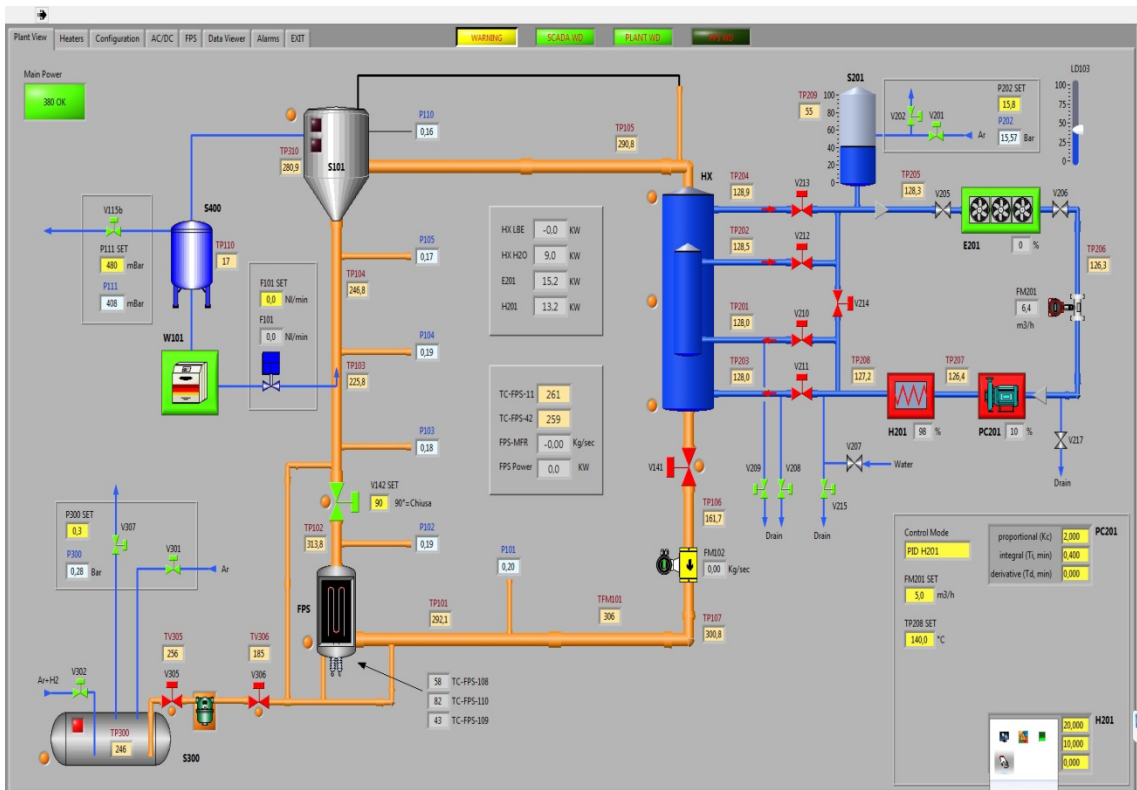
Figure.15: Remote control panel of the NACIE-UP facility

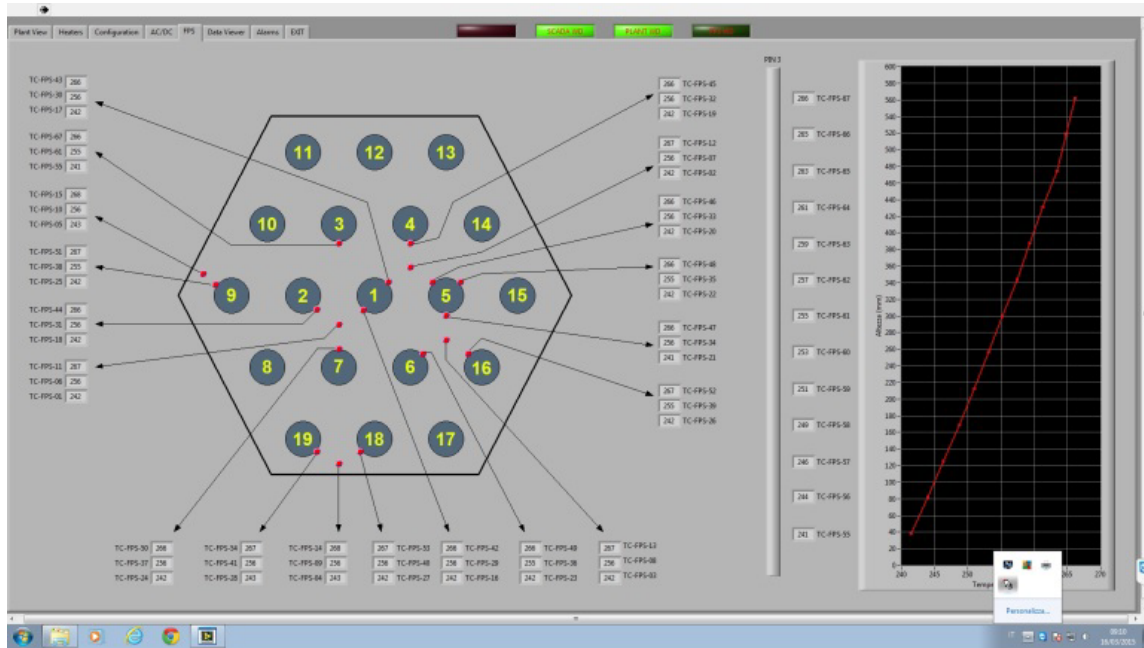*Figure.16: Control panel of the Fuel Pin simulator power*

Figure.17: Monitoring panel of the FPS temperatures.

- ## EXPERIMENTAL TEST MATRIX

The experimental campaign planned at ENEA with the NACIE-UP facility is set in the frame of the research activities to support the development of the MYRRHA irradiation facility (SCK-CEN). The FPS test section, described in Sections ▯o and ▯o, was appropriately manufactured to simulate the thermal-hydraulic behavior of a wire-spaced fuel pin bundle cooled by heavy liquid metal.

The aim of the experimental campaign is to obtain primarily stationary conditions in the facility and to characterize each stationary condition with respect to the local heat transfer measurements in the bundle, the mass flow rate, the pressure drop.

The experimental test matrix range to be performed in the next NACIE-UP campaign was provided by SCK-CEN. The expected test matrix included different power levels. For each power level, different mass flow rates are foreseen. Moreover, in the original SCK-CEN matrix in [9] most of the cases are repeated with two inlet temperatures: T_{inlet}=200, 270 °C. Nevertheless, as a first approximation, inlet temperature was not regarded, being the thermal-fluid dynamic behavior of the bundle independent by T_{inlet}.

The reference quantities for each test are: the average subchannel velocity u_{sc} [m/s], which characterize the flow from an hydraulic point of view, and the average linear power in a single pin Q_{lin} [kW/m], which defines the heat transfer boundary conditions. The subchannel velocity u_{sc} determines, on the base of the geometry of the bundle and on the fluid properties, the LBE mass flow rate in the MYRRHA FA $\dot{m}_{FA}$ [kg/s], and the LBE mass flow rate in the NACIE-UP bundle $\dot{m}_{NACIE}$ [kg/s], depending on the flow area of the fuel assembly On the other side, the linear power density Q_{lin} [kW/m] fixes the total power of the NACIE-UP 19-pin bundle Q [kW].

The range of parameters expected in the experimental test matrix provided by SCK-CEN is reported in Table.*4*

Table.4: Range of parameters for the expected test matrix provided by SCK-CEN.

FLOW REGIME	$u_{sc}[m/s]$	$\dot{m}_{FA}$ [kg/s]	$\dot{m}_{NACIE}$ [kg/s]	$\Delta T[°C]$	$Q_{NACIE}[kW]$	$Q_{lin}[kW/m]$
NC	$0.05 - 0.30$	$2.30 - 11.70$	$0.4 - 1.8$	50-230	10-35	$0.9 - 2.9$
FC	$0.13 - 0.80$	$5.00 - 31.00$	$0.9 - 5.4$	30 - 210	22 - 110	$1.9 - 9.5$

For the NACIE-UP facility, the range of mass flow rate that can be in the achieved in pure natural circulation flow is $\dot{m}_{NACIE} \approx 0.5 - 1.5 \, kg/s$, which corresponds to subchannel velocities $u_{sc} \approx 0.1 - 0.25 \, m/s$. The range of subchannel Reynolds number in this case is $\text{Re}_{sc} \approx 2000 - 5000$.

In the regime of enhanced circulation, the gas injection system provides additional pressure head and allows to achieve mass flow rates up to $\dot{m}_{NACIE} \approx 6 \, kg/s$, corresponding to subchannel velocities up to $u_{sc} \approx 0.9 \, m/s$. The maximum value of subchannel Reynolds number achievable is of about $\text{Re}_{sc} \approx 20000$.

Reynolds number range and subchannel velocities reproducible in NACIE and power range of the heaters agrees with the range required in the MYRRHA HTC specifications document by SCK.

In the NACIE-UP facility, both the bundle and the Heat Exchanger are designed for a maximum power of ~250 kW. Therefore, stationary conditions can be reached in the limits $\dot{m}_{NACIE} < 6\ kg/s$, $Q < 250\ kW$. This theoretical range is limited by the maximum clad temperature to safely operate the electrical pin $T_{clad} < 550\text{-}600\ °C$. The Fuel Pin Simulator is operated with a fuel pin protection system which automatically switches off the electric power when at least one of the wall temperatures exceeds the chosen limit. The T_{clad} limit criterion is practically satisfied if the temperature drop across the bundle is $\Delta T < 250\ °C$, and this implies a maximum power to the bundle $Q_{max} = \dot{m}_{NACIE} c_p \Delta T_{max}$ as a practical criterion for the operation of NACIE-UP.

The experimental test matrix performed considers a range power level included between 10 and 110 kW. It corresponds to linear power between 0.9 and 10 kW/m. For each power level, several mass flow rates are taken into account. At first, the case in pure natural circulation flow is attempted. Then, other tests, at lower mass flow rate are essayed, through a partial closure of the valve V142. Additional tests are performed at higher mass flow rates, by setting different flow rates of the gas injected in the riser of the primary system, just downstream the FPS test section. The experimental test matrix with all the cases performed is reported in Table.5. Reynolds and Péclet numbers in Table.5 are computed from the average temperature in the fuel bundle.

Table.5: Experimental test matrix of the performed cases.

PEC TEST NUMBER	Q[kW]	$m_{NACIEUP}$[kg/s]	$m_{MYRRHAFA}$[kg/s]	$Re_{sc}\cdot10^{-3}$	Pe_{sc}
P99	11	2.92	16.7	7.08	236
P100	11	2.28	13.07	5.45	188
P11X0	11	1.06	6.10	2.72	84
P102	11	0.72	4.08	1.93	55
P102b	11	0.68	3.86	1.84	51
103	11	0.36	2.07	1.13	26
P202	20	4.17	23.92	10.65	332
P203	20	3.10	17.86	8.09	245
P20X0	20	1.49	8.58	4.01	116
P204	20	0.73	4.20	2.24	52
P28X0	28	1.17	6.74	3.69	83
P212	36	3.33	19.18	10.06	242
P213	36	2.22	12.79	6.88	159
P214	36	1.15	6.62	3.96	77
P217	43	3.2	18.43	9.98	228
P218	43	2.8	16.13	8.75	199
P43X0	43	1.62	9.33	5.35	111
P223	52	3.40	19.47	10.81	237
P224	52	2.24	12.79	7.44	151
P265	54	3.23	18.49	10.21	226

P269	**108**	**3.95**	22.69	14.15	256

In Figure.*18* all the performed and expected cases are reported. Green and red circles represent all the cases performed. For the performed tests, the power goes between 11 and 108 *kW.* For cases at lower power, tests at pure natural circulation are performed (green circles). The cases on the left of the natural circulation curve (green line) are performed with valve V142 partially closed. For the remaining cases, the gas-lift system is active and set at several mass flow rates. White squares denote all the cases foreseen. Many other tests at pure natural circulation are expected for power level up to ~ 55 *kW.*

It should be pointed out that the behavior both of the V142 and of the gas system is highly non-linear. For this reason is not easy to predict the limits of these system to obtain the desired value of the mass flow rate. In particular, the gas lift system seems to be less efficient than expected. So, it could be hard to obtain LBE mass flow rates higher than 6 *kg/s.*

Due to its non-linear characteristic, the closure of valve V142 is almost negligible below *50-60 °.* On the other hand, the flow area becomes too narrow over *80°.* For this reason, the feasibility of the case at very low mass flow rate could be compromised.

Moreover, due to the maximum cladding temperature limits, few cases, for whom the expected temperature across is about 200-250 *°C*, could be not feasible.
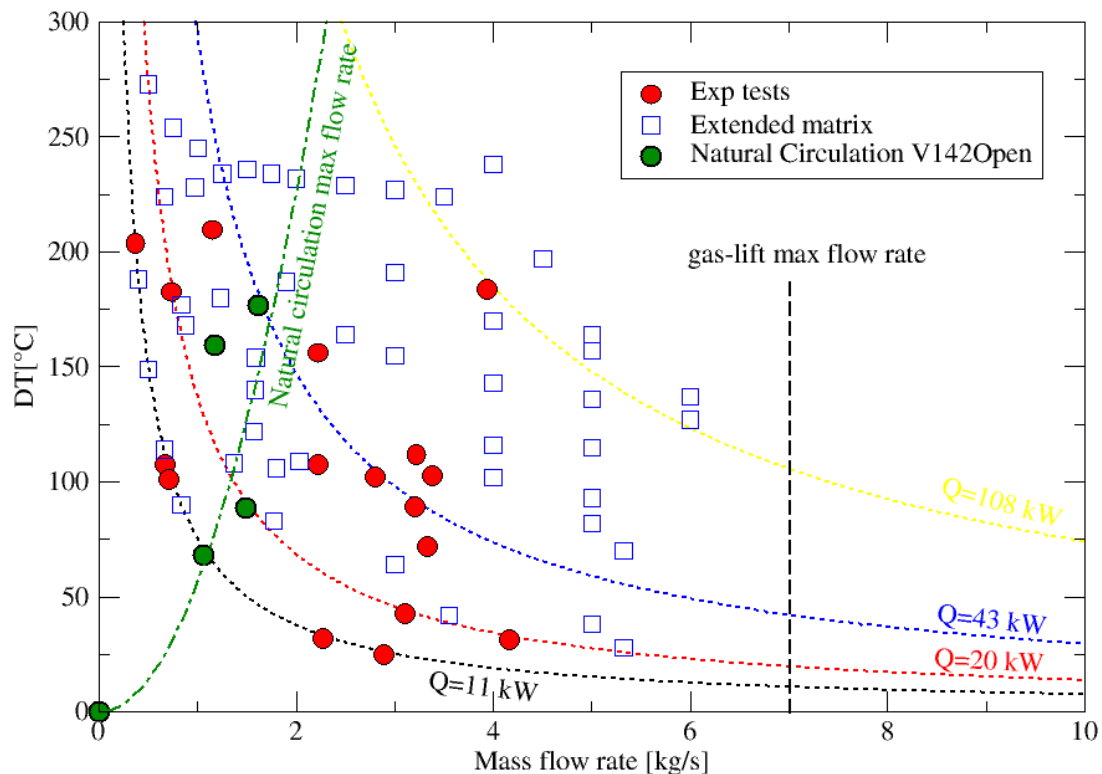

Figure.18: Test matrix with performed cases and expected cases, temperature difference across the bundle against overall mass flow rate.

The transition towards the desired conditions is started from the enhanced circulation regime. At the beginning of the test, the gas lift system is switched on and the power set to the required level. Then,

the secondary system is operated in order to find an equilibrium with the primary one. In particular, temperatures across the air-cooler (E201) and across the Heat Exchanger are checked. The ultrasonic flow meter FM201 measures the mass flow rate of the secondary water and allows to calculate the removed power. Possible disequilibrium in the secondary system can be fit with the aid of the pre-heater (H201). Nevertheless, due to its considerable inertia, the secondary system is not difficult to manage.

For the cases at natural circulation flow, the gas system is turned off after that the temperatures in the primary and secondary circuits are quite stable. From then on, a new equilibrium is sought in the system. Temperature difference across the fuel bundle and the heat exchanger increases. If necessary, adjustments in the secondary system are executed. The primary system is not modified in any way. *Figure.19* shows the temperatures trend inside the primary circuit of NACIE during the transition from enhanced to natural circulation flow for the case *P11X0*. To have an idea, each division in the time horizontal scale is 10 min.

For the cases in enhanced circulation, the mass flow rate of the gas-lift system and, in case, the V142 position, are adjusted in order to modify the LBE mass flow rate in the primary circuit for a set power level.

Data acquisition starts when the temperatures inside the primary circuit are well established in a steady state condition. The frequency of the acquisition is 1 Hz. Each test lasts about 15-20 min in order to collect a set of data statistically stationary (900-1200 samples).
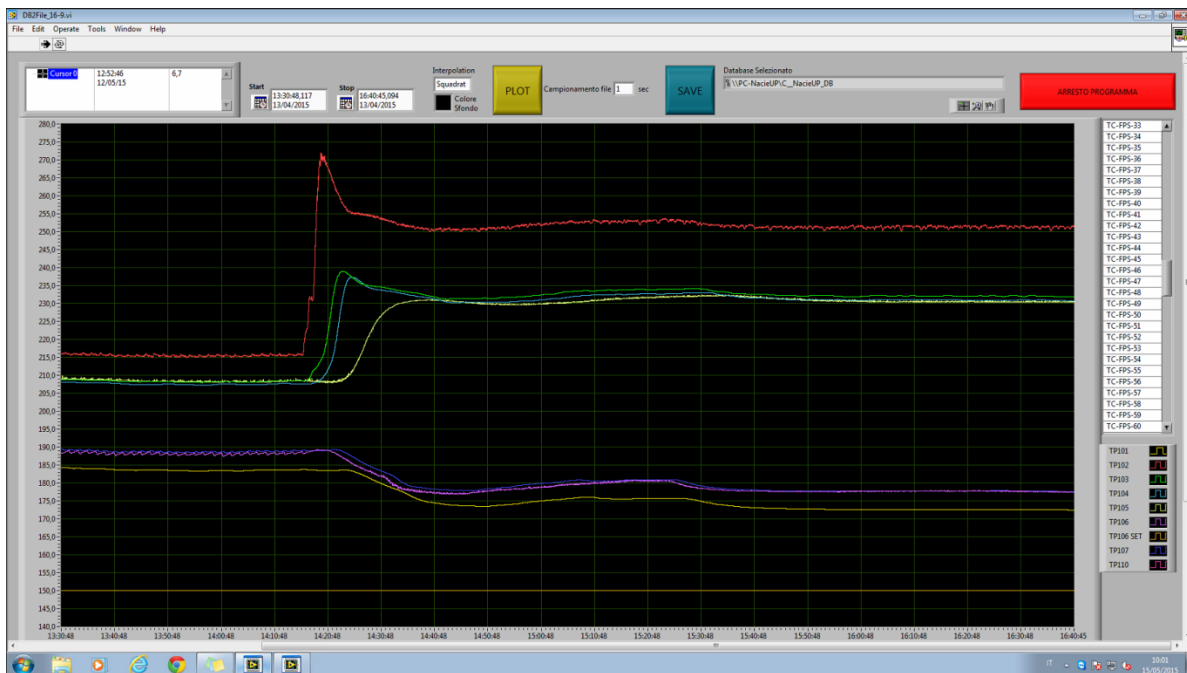

Figure.19: LBE temperature trends in during the transition from enhanced to natural circulation regimes, in the NACIE-UP facility..

- ## POST-PROCESSING METHOD

The main objective of this work is the characterization of the thermal hydraulic phenomena involved inside the MYRRHA fuel bundle in specified conditions. For this purpose, appropriate instrumentation was provided and described in Section ▯o.

Nevertheless, acquired data cannot be used raw as acquired to obtain the derived quantities, but need appropriate treatment before being used. In fact, the set of the acquired data are affected by statistical and instrumentation errors. Then, some derived quantities are computed from measured data. All the variables adopted in the analysis of the experimental tests will be defined in Section ▯o.

Further, methods considered for the uncertainties analysis and error propagation for derived quantities will be described in the next Sections.

Some more information about the implementation of the post-processing methods in a Matlab routine will be summarized in Section 4. The Matlab post-processing routine is reported in **Annex A**.

- ### Definitions and derived quantities

- #### *Bulk temperature and section-averaged wall temperature*

For the experimental tests considered, the main instrumentation is the set of thermocouples located inside the fuel pin simulator. As describes in Section ▯o, a total of 67 TCs are arranged in three different sections, placed respectively *38, 300* and *562 mm* after the beginning of the heated region.

Nevertheless, there are no thermocouples just before and soon after the active region. Though, the thermocouple TP102 is located downstream the FPS, outside the test section and should give a good estimation of the bulk temperature at the outlet of the bundle. For this reason, the temperatures at the inlet and at the outlet of the heated region of the FPS (T_{in} and T_{out}) were obtained by linear extrapolation of the LBE bulk temperature measured in section A (38 *mm* after the beginning of the active zone) and section C (38 *mm* before the end of the active zone). It should be stressed that sections A and C are very close respectively to the inlet and outlet section of the active region of the FPS, which is *600 mm* long.

Then, the LBE temperatures across the heated length are used to obtain the LBE mass flow rate inside the loop. In fact, during the experimental campaign, the induced mass flow meter was not available for operation. For this reason, a correct evaluation of the LBE temperatures across the fuel pin bundle is envisaged.

The bulk temperature at the monitored sections need to be estimated from the measured points. Since these points are not homogeneously distributed inside the section, the arithmetic average temperature is not correct. A weighted average temperature is carried out instead. The 5 bulk thermocouple placed in each of the three sections monitored are multiplied for weighting factors. Weighting factors take into account the relative importance of the flow area represented by the subchannel where the thermocouple is located.

The section bulk temperature is defined as in equation (8):

$$\overline{T}_{bulk} = T_{b\,S2} \cdot w_2 + T_{b\,S5} \cdot w_5 + T_{b\,S22} \cdot w_{22} + T_{b\,S26} \cdot w_{26} + T_{b\,S33} \cdot w_{33} \qquad (8)$$

Weighting factors are defined in Table 6.

Table.6: Weights to compute section-averaged temperatures for the monitored sections.

w_2	w_5	w_{22}	w_{26}	w_{33}
0.058	0.058	0.346	0.179	0.359

Weights w_2 and w_5 are equal and such that their sum is representative of the flow area of the central rank. w_{22} account for the total flow area of the second rank. The sum of w_{26} and w_{33} represent the flow area of the external rank and are divided with respect to the shape of the subchannel. Similarly, the section-averaged wall temperature was defined, as in equation (9)

$$\overline{T}_{wall} = T_{w\,S2} \cdot w_2 + T_{w\,S5} \cdot w_5 + T_{w\,S22} \cdot w_{22} + T_{w\,S26} \cdot w_{26} + T_{w\,S33} \cdot w_{33} \qquad (9)$$

The wall temperature for each subchannel, (e.g., $T_{w\,S2}$ for subchannel S2) is arithmetic averaged among the wall temperature related to that subchannel.

▪ *Temperatures across the FPS*

As mentioned before, the section-averaged bulk temperature at sections A and C was used to obtain the temperature at the inlet and outlet of the FPS through a linear extrapolation.

Figure.20 shows the values of the section-averaged bulk temperatures at the three sections and the extrapolated values across the heated length. The bulk temperature at section B is almost overlapped to the linear trend between sections A and C. This agreement justifies the linear assumption and the method chosen to find out T_{in} and T_{out}.
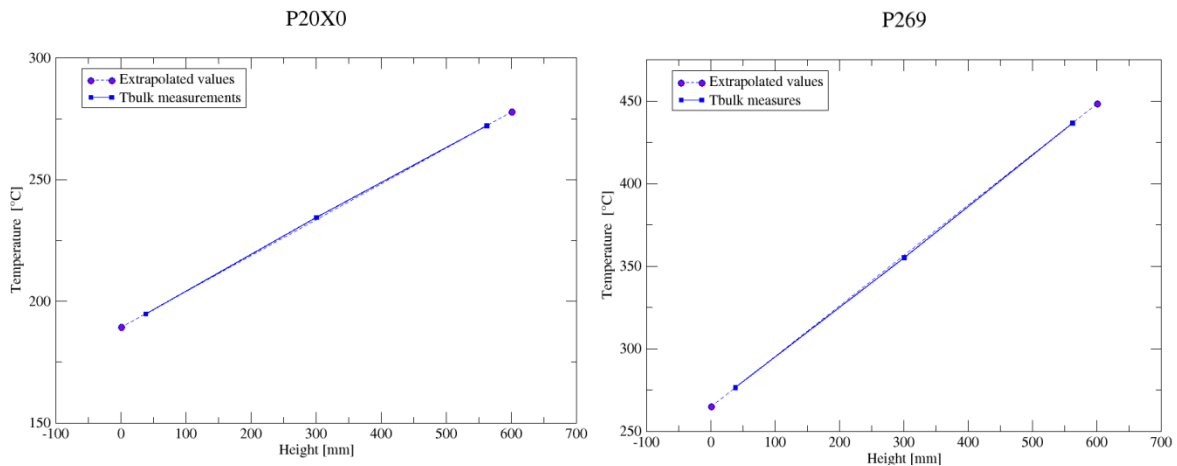

Figure.20: LBE average bulk temperature measured at three reference sections and extrapolated values for T_{in} and T_{out}.

After that, all the values of the T_{out} were compared with the LBE temperature measured by TP102. The comparison is reported in *Table.7*. In the worst case the difference between the two temperatures is always below 5°C and less than 1 °C in most cases. The good agreement provides

good arguments for the linear extrapolation method to obtain the temperature across the bundle. Moreover, it legitimates the weighted average definition for bulk and wall temperatures in the overall section.

Table.7:Comparison between temperature at FPS outlet obtained from linear extrapolation and measurement of TP102 downstream the test section.

Test	T_{out} FPS calcualted [°C]	TP102 measurements [°C]	Difference [°C]
P11X0	253.9	251.3	2.6
P20X0	277.8	277.7	0.1
P28X0	374.6	374.9	-0.3
P43X0	403.1	404.1	-1
P099	217.2	215.4	1.8
P100	214.2	213.5	0.7
P102	288.1	284.9	3.2
P102b	294.7	292.1	2.6
P103	393.8	389.1	4.7
P202	234.1	233.9	0.2
P203	245.7	245.7	0
P204	374.3	371.6	2.7
P212	313.2	311.2	2
P213	341.3	339.4	1.9
P214	439.5	439.0	0.5
P217	335.3	333.1	2.2
P218	342.3	342.7	-0.4
P223	352.5	354.8	-2.3
P224	400.1	402.8	-2.7
P265	354.6	355.8	-1.2
P269	448.5	449.4	-0.9

▪ *Wall temperature correction*

Wall temperatures are measured by embedded thermocouples, placed inside the cladding, in a groove 0.38 *mm* deep. The TCs diameter is 0.35*mm*. Therefore, wall TCs measures the temperature in a position slightly inside the clad, which is higher than at the clad outer surface.

The correction is implemented by applying the heat conduction law in cylindrical geometry, as described in equation (10)

$$T_w = T_{ac} - \frac{Q}{2\pi N L_{active} k_{ss}} \ln\left(\frac{D/2}{D/2 - \delta_g}\right) \qquad (10)$$

where T_{ac} is the acquired temperature, N is the number of pins in the bundle, k_{ss} is the conductivity of stainless steel at T_{ac}, and δ_g is the distance between the center of the TC and the cladding outer surface.

As the differences between bulk and wall temperature are very small, due to the good heat transfer properties of the LBE, this correction is important for a correct estimation of the Nusselt number. To have an idea of the importance of this correction, the Biot number (Bi) was calculated for the distance δ_g. Biot number for the extrapolation distance is defined in equation (11):

$$\text{Bi}_{extr} = \frac{h_{avg} \cdot \delta_g}{k_{ss}} \qquad (11)$$

The Biot number represents the ratio between the thermal resistance in the wall and in the boundary layer of the fluid. For Bi<<1, the temperature drop is all in the boundary layer, and the TC extrapolation error is not important. *Table.8* reports the Biot number for the extrapolation distance δ_g for all the cases at the three monitored sections. In this case, the heat transfer coefficient h_{avg} is calculated from section-averaged temperatures:

$$h_{avg} = \frac{q''}{\left(\overline{T}_{wall} - \overline{T}_{bulk}\right)} \qquad (12)$$

In most cases 20% of the temperature drop occurs inside the extrapolation distance. In one case the Biot number even goes up to 0.32. If this temperature jump is not considered to occur inside the clad but is incorporated inside the convective heat transfer term, significant errors are made in the analysis of the heat transfer phenomena. It must be noticed that the Biot number is larger at larger mass flow rates where the TC correction factor will be higher.

Table.8: Biot number for the extrapolation distance at three section.

Case	Power [Kw]	Bi_{extr} section A	Bi_{extr} section B	Bi_{extr} section C
P11X0	11	0.22	0.17	0.19
P20X0	20	0.20	0.18	0.15
P28X0	28	0.19	0.17	0.15
P43X0	43	0.19	0.18	0.15
P099	11	0.32	0.23	0.25
P100	11	0.24	0.18	0.17
P102	11	0.20	0.16	0.18
P102b	11	0.19	0.16	0.18
P103	11	0.18	0.16	0.18
P202	20	0.29	0.26	0.20
P203	20	0.25	0.23	0.18
P204	20	0.17	0.16	0.14
P212	36	0.23	0.20	0.28
P213	36	0.21	0.18	0.21
P214	36	0.18	0.16	0.14
P217	43	0.24	0.21	0.27
P218	43	0.22	0.21	0.18

P223	52	0.25	0.23	0.18
P224	52	0.22	0.18	0.16
P265	54	0.23	0.21	0.19
P269	108	0.24	0.21	0.21

- *LBE Mass flow rate*

As stated before, T_{in} and T_{out} are used to compute the LBE mass flow rate inside the primary loop, since the mass flow meter is currently unavailable. The mass flow rate is calculated through the thermal balance across the heated length of the test section. Nevertheless, at least 3% of the nominal power is released outside the active region, so just the 97% of nominal power is considered for the thermal balance. This efficiency factor was provided by Thermocoax [10] and it is consistent with the pin internal features.

Thus, mass flow rate is obtained through the following equation:

$$\dot{m} = \frac{0.97 \, Q_{nom}}{\overline{c}_p (T_{out} - T_{in})} \qquad (13)$$

where $\overline{c}_p$ is the LBE specific heat at average temperature between FPS inlet and outlet.

- *Non-dimensional numbers*

Some non-dimensional numbers were used in order to analyze the experimental data and characterize the thermal-hydraulic behavior of the fuel pin bundle representative of the MYRRHA subassembly.

In our analyses the Reynolds number was calculated as stated in equation (14). *Re* at the monitored sections is calculated form the dynamic viscosity of the section-averaged bulk temperature $\overline{T}_{bulk}$.

$$\mathrm{Re} = \frac{\dot{m} \, D_h}{A_{bundle}\mu} \qquad (14)$$

Prandtl number is reported in equation (15). Also in this case LBE properties are calculated at temperature $\overline{T}_{bulk}$.

$$\mathrm{Pr} = \frac{\mu \, c_p}{k} \qquad (15)$$

Peclét number is directly obtained from the Reynold and Prandtl numbers:

$$\mathrm{Pe} = \mathrm{Re} \cdot \mathrm{Pr} \qquad (16)$$

The non-dimensional number for the heat transfer analysis is the Nusselt number. It is defined as in equation (17), where L represents the characteristic length in the phenomenon under consideration and *k* is the fluid conductivity.

$$Nu = \frac{h \, L}{k} \qquad (17)$$

In this work, different definitions to refer to the Nusselt number are provided.

At first, the local definition is contemplated and it is reported in equation (18). In this case, the local values of temperature $T_{w\,sc}$ and $T_{b\,sc}$ are taken into account to calculate *h*. $T_{b\,sc}$ is the bulk temperature for the single subchannel and $T_{w\,sc}$ is the average among the wall TCs related to that subchannel. k_{LBE} is the LBE conductivity at the temperature $T_{b\,sc}$.

$$Nu_{sc} = \frac{q"}{\left(T_{w\,sc} - T_{b\,sc}\right)} \cdot \frac{D_h}{k_{LBE}}$$

(18)

Then, two average Nusselt number are defined.

The first one follows equation (17) and uses the section averaged temperature $\overline{T}_{wall}$ and $\overline{T}_{bulk}$ to obtain the heat transfer coefficient *h*. Its definition is reported in equation (19). In the following, it will be mentioned as Nu_1. In this case k_{LBE} is the LBE conductivity at the temperature $\overline{T}_{bulk}$.

$$Nu_1 = \frac{q"}{\left(\overline{T}_w - \overline{T}_b\right)} \cdot \frac{D_h}{k_{LBE}}$$

(19)

The second one is defined as the weighted average of the local (subchannels) Nusselt number (see equation (20). The weighting factors are the same defined in *Table.6*. It will be referred to this definition as Nu_2.

$$Nu_2 = Nu_{S2} \cdot w_2 + Nu_{S5} \cdot w_5 + Nu_{S22} \cdot w_{22} + Nu_{S26} \cdot w_{26} + Nu_{S33} \cdot w_{33}$$

(20)

Results for the local values of the Nusselt number obtained from the experimental data are reported in detail in the next sections. A comparison between the two definitions for the average values is discussed later. Here, it must be stressed that the two definitions are conceptually different being

$$\overline{\left(\frac{1}{\Delta T}\right)} \neq \frac{1}{\overline{\Delta T}}.$$

o **LBE physical properties**

The estimation of the non-dimensional numbers, mentioned in the previous section, requires the knowledge of the LBE physical properties, which are all temperature-dependent.

In our work, these properties were evaluated using empirical correlations in the OECD/NEA Handbook on LBE properties [11].

LBE density is estimated by a linear function of temperature, following equation (21). This function approximates some selected data from literature with a standard deviation which does not exceed 0.8%.

$$\rho_{LBE} = 11096 - 1.3236 \cdot T \qquad (21)$$

As stated in [11], available data on the heat capacity of LBE are very limited. For these data, a parabolic polynomial trend is extrapolated, in the temperature range of 400-1100 K. The standard deviation of the correlation with respect to the experimental data is below 5%.

$$c_{p\,LBE} = 159 - 2.72 \cdot 10^{-2} \cdot T + 7.12 \cdot 10^{-6} \cdot T^2 \qquad (22)$$

The LBE dynamic viscosity can be described by the fitting correlation in equation (23) $\mu_{LBE} = 4.94 \cdot 10^{-4} \exp\left(\dfrac{754.1}{T}\right)$. The maximum difference between the LBE viscosity given by the correlation and the database set is about 5%.

$$\mu_{LBE} = 4.94 \cdot 10^{-4} \exp\left(\frac{754.1}{T}\right) \qquad (23)$$

As it regards the LBE conductivity, some differences exist between Western and Russian data set [11]. Considering some selected data correlation in equation (24) was obtained. The standard deviation from Ida (1988) data is about 5%.

$$k_{LBE} = 3.61 + 1.517 \cdot 10^{-2} \cdot T - 1.741 \cdot 10^{-6} T^2 \qquad (24)$$

o **Error analysis method**

In this work, several sources of uncertainties are considered. First of all, the statistical error lead to the sampling must be taken into account. All the measured data are also affected by the errors due to the instrumentation. For this reason, the total uncertainties for each acquired variable is the same as computed in equation (25).

$$\sigma_{Xi,tot}^2 = \sigma_{Xi,stat}^2 + \sigma_{Xi,instr}^2 \qquad (25)$$

Another source error in the post-processing method is the uncertainty connected to the computation of the physical properties through the correlation mentioned in Section ⬚o.

Following the error propagation theory , the uncertainties of a derived quantity Y ,which is function of n variables X_i (26), can be computed from the standard deviation of the n variables, following equation (27).

$$Y = f\left(X_1, ..., X_n\right) \qquad (26)$$

$$\sigma_Y^2 = \sum_{i=1}^{n} \left(\frac{\partial f}{\partial Xi} \cdot \sigma_{Xi}\right)^2 \qquad (27)$$

In this work, the calculation of the uncertainties of the experimental data and the derived quantities was accomplished through the numerical means. This method is implemented in a Matlab routine, specifically for all the post-processing calculations, reported in the following.

1. For each variable, the acquired data (900-1200 samples) are read from the post-processing routine.
2. In order to consider the instrumentation uncertainty, a random value is added to each sample of the considered variable. This random value is chosen inside a Gaussian distribution with a standard deviation equal to the error of the instrumentation. It is proved that, for a large number of samples ($n_{samples}$ >1500), the results are no more affected by the number of samples. As a consequence, the added random value does not affect the average value of the real quantity and the standard deviation coincides with the instrument error. In our application, the acquired data includes a statistical error. So, once this method is applied to the acquired data, the resulting error is the total error, as defined in (25).
   The same method is applied to take into consideration the statistical error in the correlation used to compute the LBE physical properties.
3. The derived quantities are computed form the acquired data (which now comprise all the sources of errors). These quantities are computed as vectors with a length of the number of samples.
4. The average value and the standard deviation of the derived quantity are calculated. The standard deviation of the derived quantity is proved to be the same as it would have been calculated with equation (27).

- ## RESULTS: HEAT TRASFER ANALYSIS

In this chapter the experimental results are presented. Many details about acquired and derived quantities, for some test cases of the present experimental campaign, are presented in other deliverables [4] and [12]. In these two works, the thermal-hydraulic parameters of the tests considered, detailed temperature trends inside the FPS and some information about the heat transfer are presented for the tests in mixed [4] and free [12] convection.

In the present work, a more comprehensive analysis on FPS behavior is presented. In particular, the heat transfer coefficient is regarded. This study is mainly achieved through the analysis of the Nusselt number, defined in different ways, which are reported previously in the document. Nusselt number is graphically reported as a function of the Péclet number ,which allow to take into consideration the hydrodynamic features of the case under examination. The analysis are carried out for the three monitored section inside the fuel bundle.

Plots on the Nusselt number versus the Péclet allow the comparison of the experimental data with the correlations existing in literature. Comprehensive review about the existing correlations for the heat transfer in heavy liquid metal were accomplished by Pfrang and Struwe (2007) [13] and by Mikityuk (2009) [14].

Among the correlation in literature, three were chosen for comparison in this work. For this purpose, it should be reminded that the bundle lattice of the FPS is characterized by a ratio $P/D = 1.28$ and the range of the experimental matrix is characterized by $Pe < 500$.

The first choice is the correlation by Ushakov (1977), reported in equation (28). According to [13], this correlation is valid in the range of $1 < Pe < 4000$ and $1.2 \leq P/D \leq 2.0$.

$$Nu = 7.55 \frac{P}{D} - 20 \left(\frac{P}{D} \right)^{-13} + \frac{3.67}{90 \cdot \left(\frac{P}{D} \right)^2} \cdot Pe^{\left(0.56 + 0.19 \cdot \frac{P}{D} \right)} \qquad (28)$$

The second one is the correlation by Mikityuk (2009), described in (29). It was obtained from four different sets of experimental data in bundle geometry. The validity range is $30 < Pe < 5000$ and $1.1 \leq P/D \leq 1.95$.

$$Nu = 0.047 \cdot \left(1 - e^{-3.8 \cdot \left(\frac{P}{D} - 1 \right)} \right) \cdot \left(Pe^{0.77} + 250 \right) \qquad (29)$$

The third correlation is from Kazimi and Carelli (1976) and in [13] is described by equation (30). It was obtained using several experimental campaigns conducted with different coolants (Na, Hg and NaK). It is recommended for the ranges $10 < Pe < 5000$ and $1.1 \leq P/D \leq 1.4$.

$$Nu = 4 + 0.16 \left(\frac{P}{D} \right)^5 + 0.33 \left(\frac{P}{D} \right)^{3.8} \cdot \left(\frac{Pe}{100} \right)^{0.86} \qquad (30)$$

Results are presented in two sections. At first, local analysis are discussed. It regards the computation of the Nusselt number for the single subchannels. It is fully discussed in Section ▯o. Then, section-averaged heat transfer will be analysed, following the different definitions described previously, equations (19) and (20). The results are displayed in Section ▯o. Other results, concerning the overall coolability of the NACIE-UP fuel bundle and the similarities with the MYRRHA fuel assembly are finally discussed later.

o **Local results**

The local Nusselt number is defined previously in the document. This definition allows to evaluate the heat transfer capability for the single subchannels and to compare results. In particular, the subchannels of the central rank are representative of the subchannel of an infinite lattice, so their behaviour is of relevant interest. Among them, two subchannels, S2 and S5, are instrumented.
Figure.21 shows all the data obtained from the experimental data for the local Nusselt. The collected points are distributed along a wide band of Nusselt for a range of Péclet $25 < Pe < 400$. Nevertheless, most of data stay between the correlations of Ushakov and Mikityuk. Another great part of the points are closer to the Carelli correlation, which predicts smaller *Nu* with respect to Ushakov and Mikityuk correlations at the same *Pe*. Very few data are set above the reference correlations. It must be stressed that the data dispersion in *Figure.21* is due to the different rank of subchannels and different measurement levels showed all together in an overall graph.
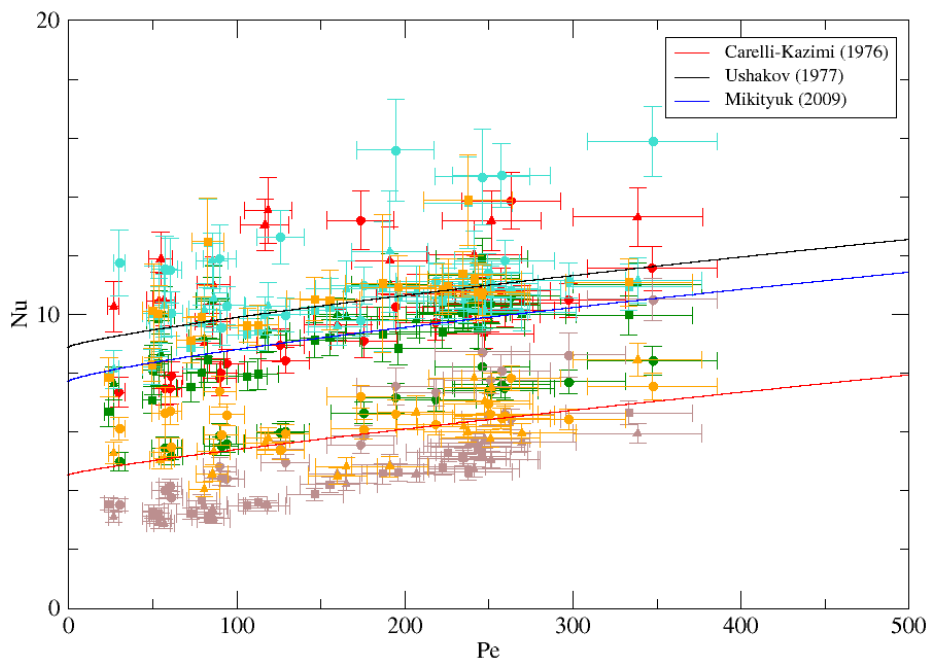

Figure.21: Local values of Nusselt number versus Péclet number for all the subchannels, all the sections and all the experimental tests.

In order to better understand the results and the general trends, the experimental points are differentiate with respect to the subchannel under considerations. From *Figure.22* to *Figure.26* the Nusselt number for the single subchannels is reported.

Figure.22 shows the results for the subchannel S2. For this channel, the experimental points at section C are not considered. In fact, in most cases the temperature differences between wall and bulk are very small, especially at very low mass flow rate. Then, the Nusselt number is strongly affected by the TCs accuracy and the obtained values could be not reliable. The plotted data set very close to the Ushakov and Mikityuk correlations. However, at low Pe, Nusselt at section A are a bit lower than in section B and also lower than the two reference correlations. For $Pe \simeq 200-300$ data for section A and B are closer and set between the Ushakov and Mikityuk correlations.
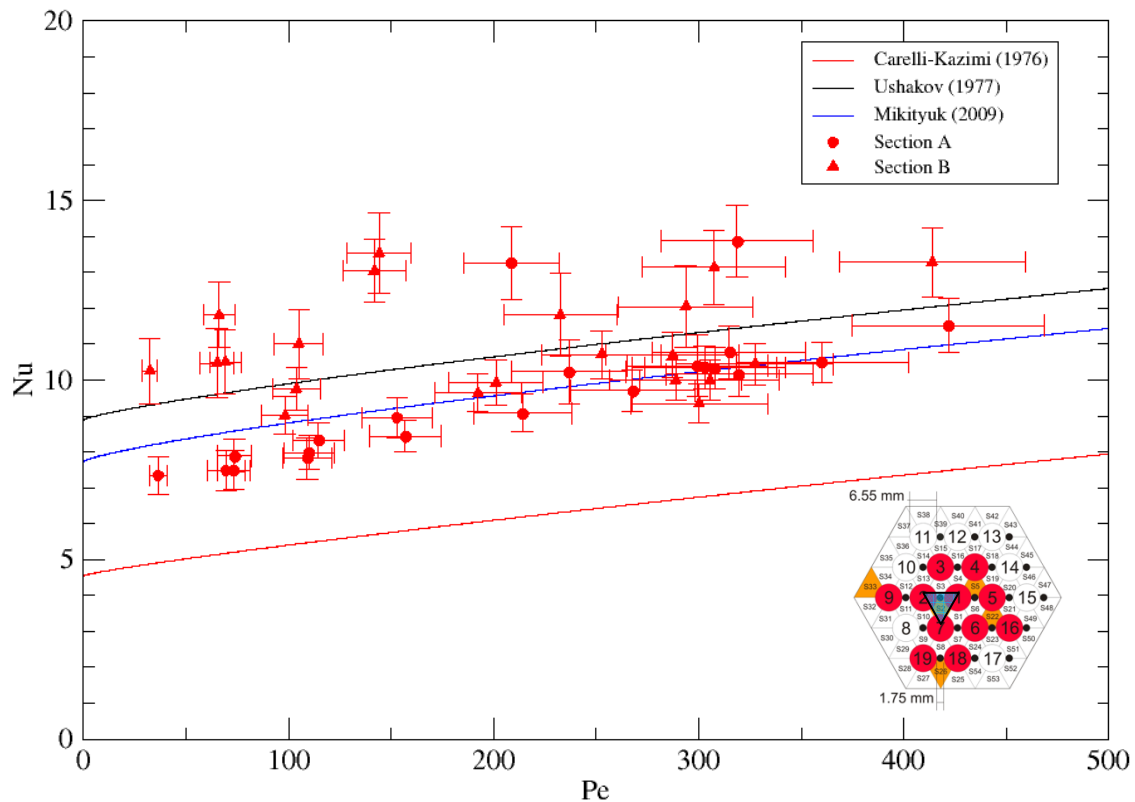

Figure.22: All experimental data of local Nusselt versus Péclet for subchannel S2.

Figure.23 reports the same results for the central subchannels S5. In this case, most of the experimental data are more or less between the two correlations which gives higher Nu. Some data set lower and are in accordance with the Carelli correlation. All the lower Nu are calculated in section A, which generally exhibits smaller Nu than in section B and C, for the subchannel S5.

Subchannel S5
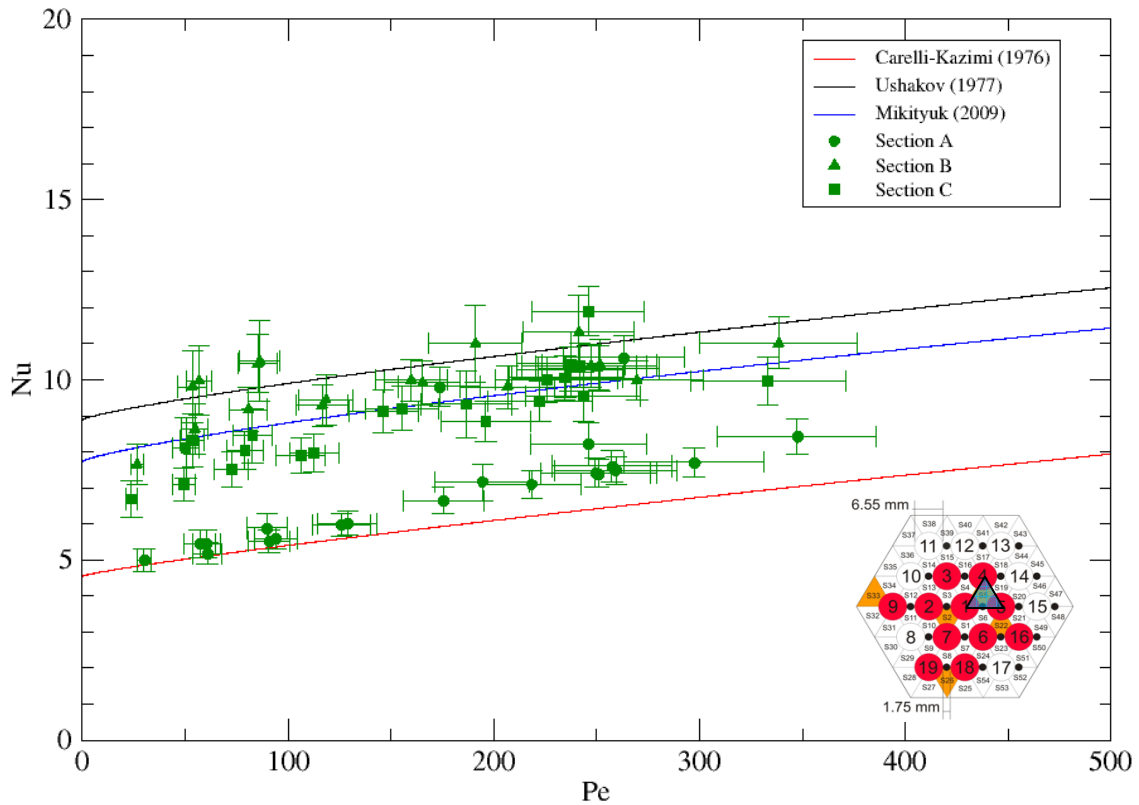
Figure.23: All experimental data of local Nusselt versus Péclet for subchannel S5.

The local values of the Nusselt number for the subchannel S22 are depicted in *Figure.24*. This subchannel is in the second rank, between the central and the external ones. The results gives generally high Nusselt numbers, which are in accordance with the Ushakov and Mikityuk correlations. Few data are quite above the correlations suggested by literature. Most of them belongs to section A.

Subchannel S22

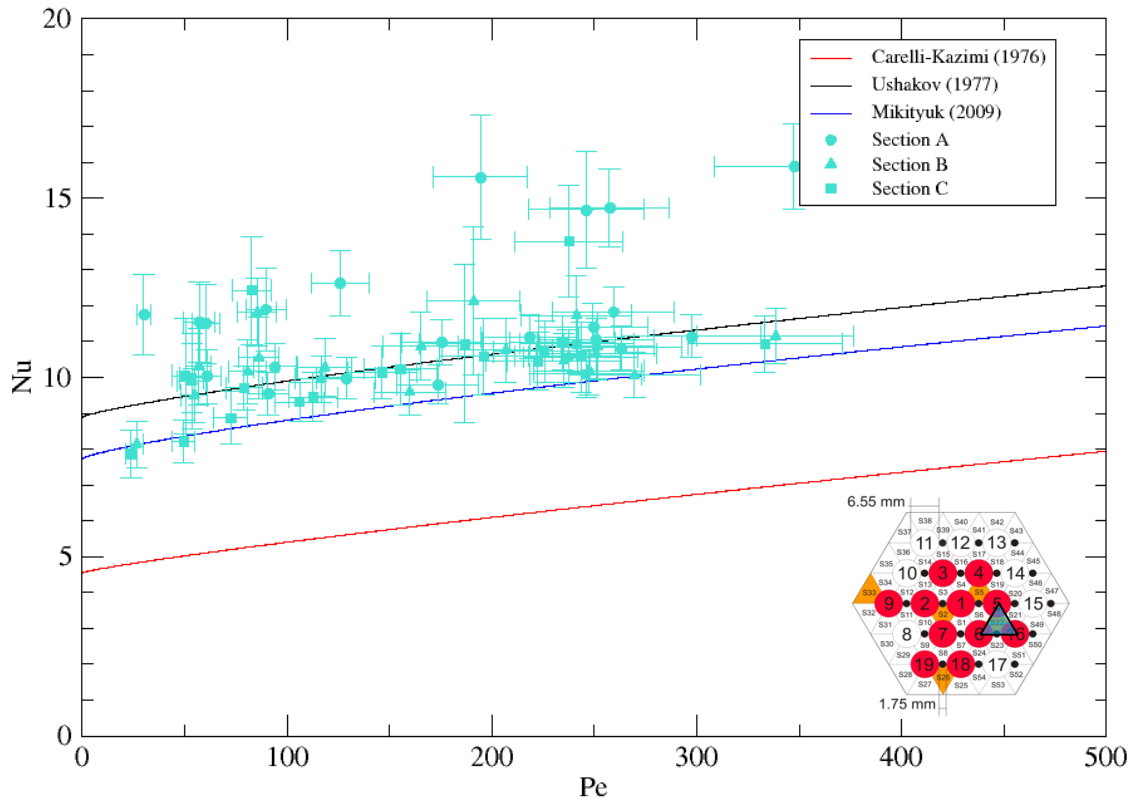*Figure.24: All experimental data of local Nusselt versus Péclet for subchannel S22.*

In *Figure.25*, the results for the subchannel S26 are presented. It should be mentioned that subchannels S26 and S33 belong to the peripheral rank. For these subchannels the thermal field is affected by the presence of the hexagonal wrap. In fact, the heat transfer to the outer structures plays a crucial role and LBE temperature is lower than in the central channels. Nevertheless, heat flux is the same in all the pin of the bundle. The temperature difference between wall and bulk increases and the Nusselt number decrease. *Figure.25* shows that the Nusselt number for subchannel 26 is generally much lower than in the internal ranks. The experimental point are even overestimated by the Carelli correlation, which is quite conservative. Nevertheless, in this case the trend is that *Nu* decreases along the active region. In fact, experimental *Nu* in section A are higher than in section B and C.

Subchannel S26
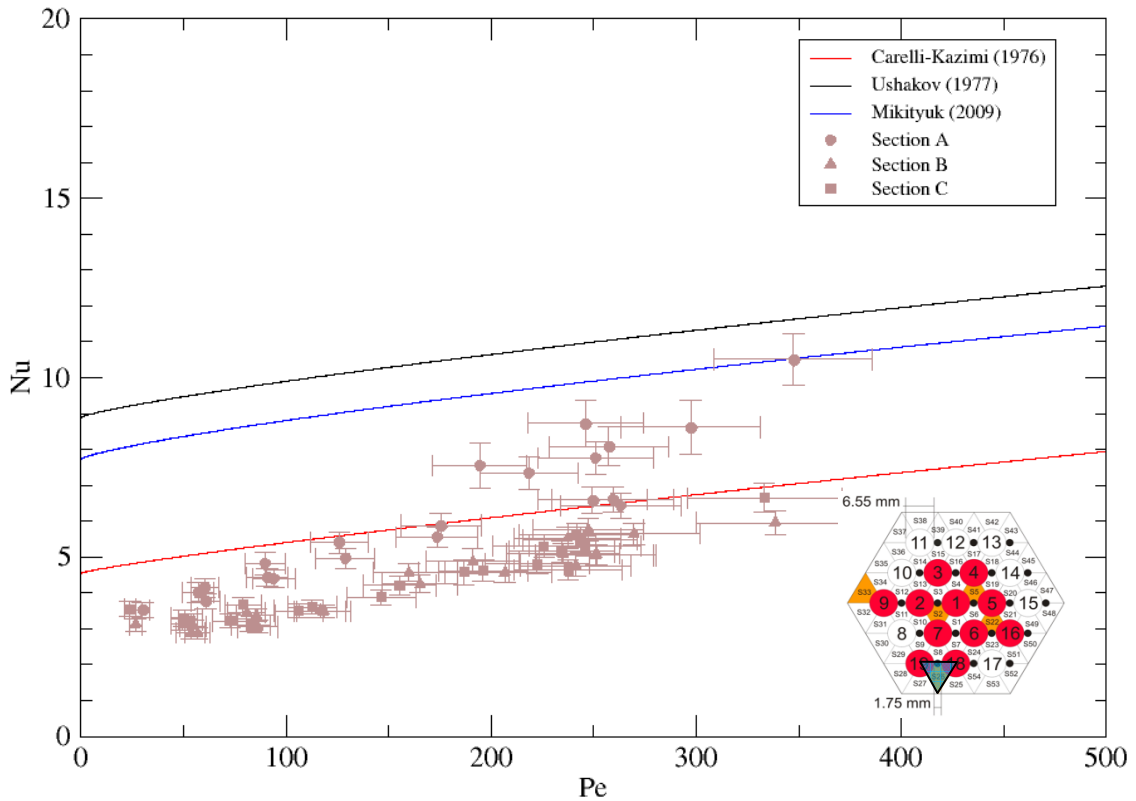
Figure.25: All experimental data of local Nusselt versus Péclet for subchannel S26.

The last monitored subchannel is S33, which is a corner subchannel. Local *Nu* versus *Pe* for S33 is displayed in *Figure.26*. With respect to subchannel S26, Nusselt number are higher and can be discerned in two zones. At section A and B, results are in accordance with the Carelli correlation, instead in section C the *Nu* increases for all the test cases and values are well represented by the Ushakov correlation.
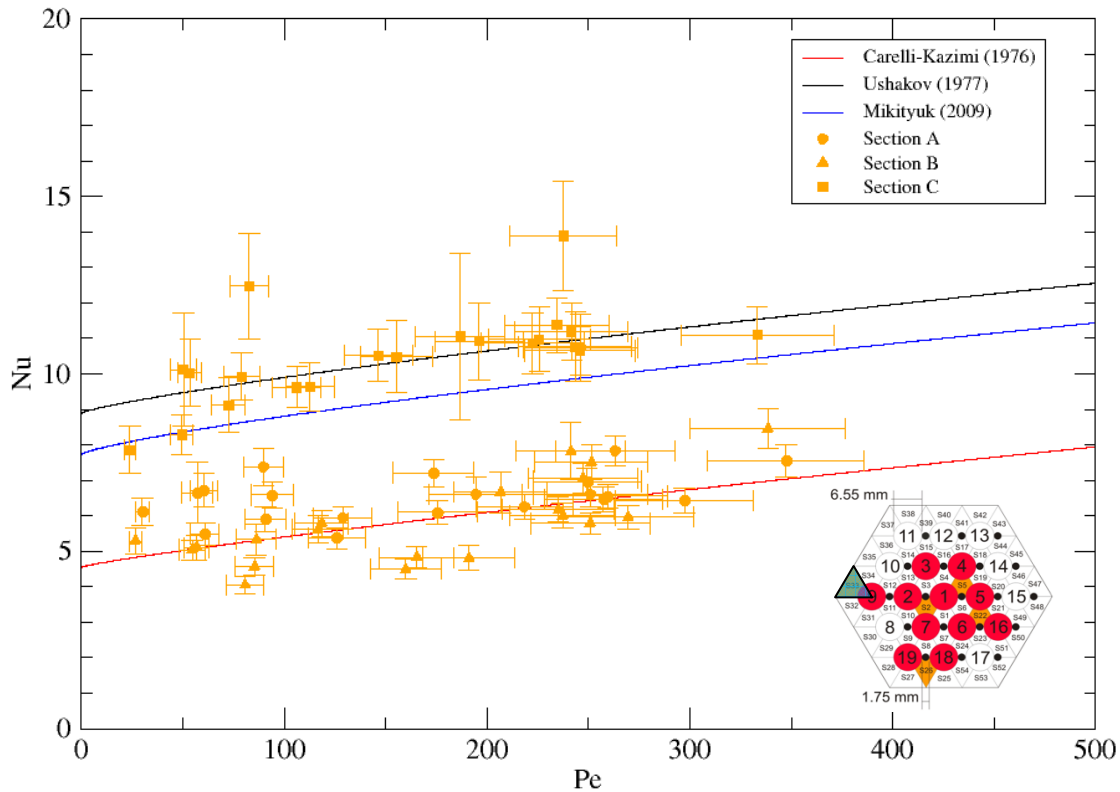
Figure.26: All experimental data of local Nusselt versus Péclet for subchannel S33.

Figure.27 reports the same results shown before but data are selected with respect to the axial location. It can be reminded that section A is located *38 mm* after the beginning of the active region, section B at *300 mm* and section C at *562 mm,* which is *38 mm* before the end of the heated region.

From these local data, a general trend of the local Nusselt number behaviour as a function of the axial position is not evident. The increasing or decreasing trend depends on the subchannel considered. Other analysis on the axial trend for the Nusselt number will be discussed for the section-averaged overall heat transfer, in next section.

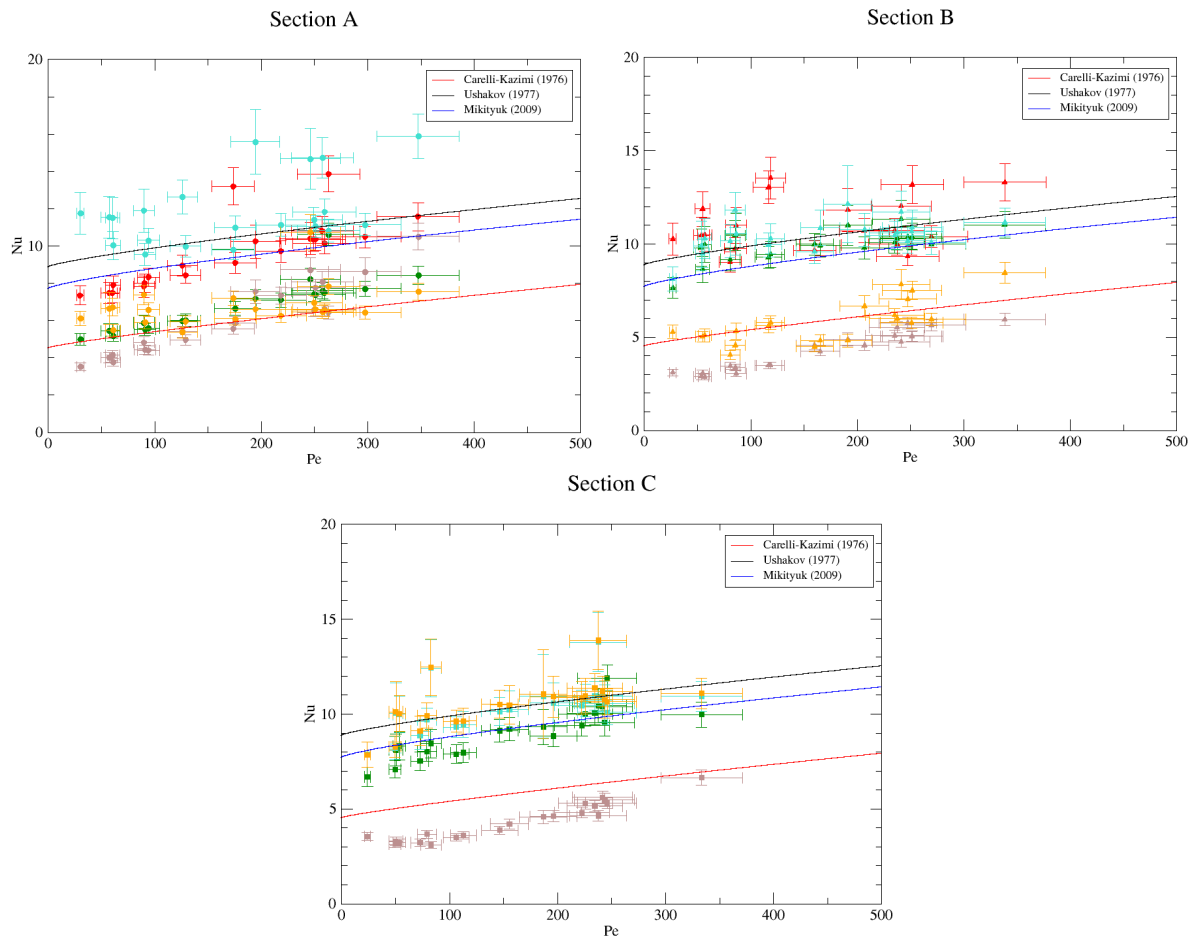Local Nusselt numbers data at the different sections are reported in table format in **Annex B**.

Section A

Section B

Section C

Figure.27: Local Nusselt number for all the test cases at the three monitored sections.

o **Overall heat transfer**

In previous Sectiona, the Nusselt number for the section-averaged analysis was defined. Results obtained from that definition are analyzed in the following.

Experimental results for the Nu_1 and Nu_2 are reported in *Figure.28*and *Figure.29*. Nu_1 is computed from the section-averaged wall and bulk temperature. The following values are generally quite low and almost all the data settle between the Carelli and the Mikityuk correlations. It is clear that this definition of Nusselt is widely affected by the colder LBE in the peripheral rank, which results in significant wall-bulk temperature differences.
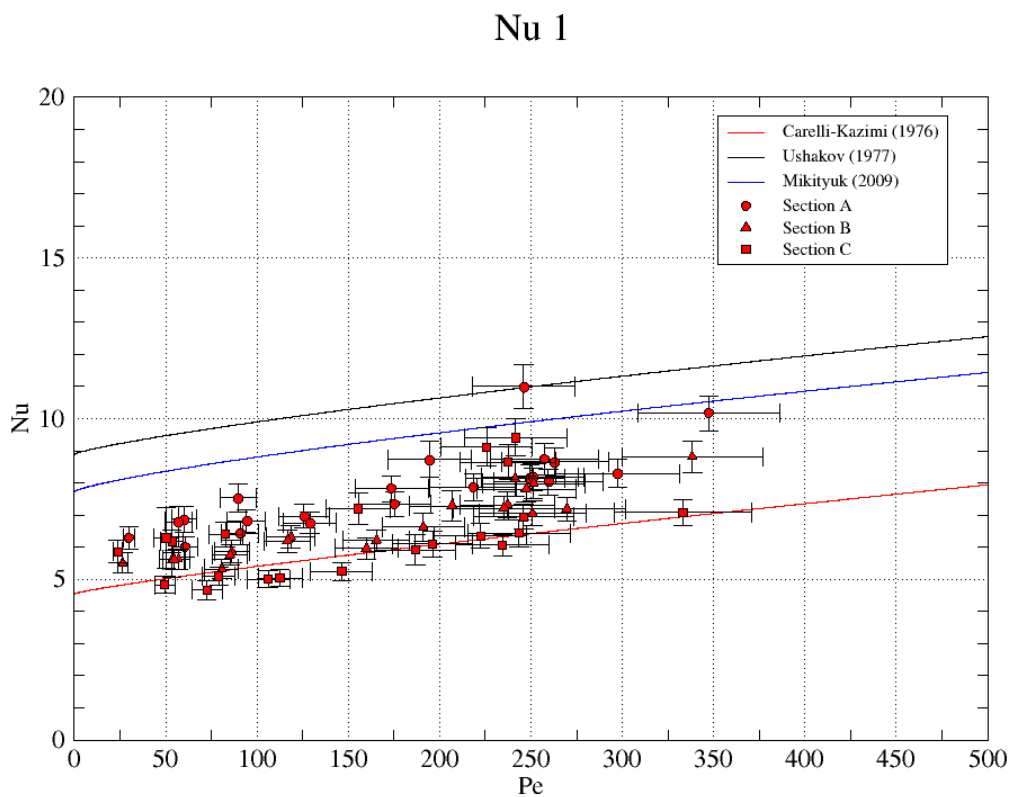
Figure.28: Section-averaged Nusselt number Nu_1 at all the sections for all test cases.

Nu_2 is computed as weighted average of the local Nusselt number. In this case, the lower local Nusselt of the peripheral rank affect less the overall Nusselt. Values of Nu_2, obtained with experimental data, are reported in *Figure.29*. Generally, these values are a bit overestimated by the Mikityuk correlation but well above the Carelli one.
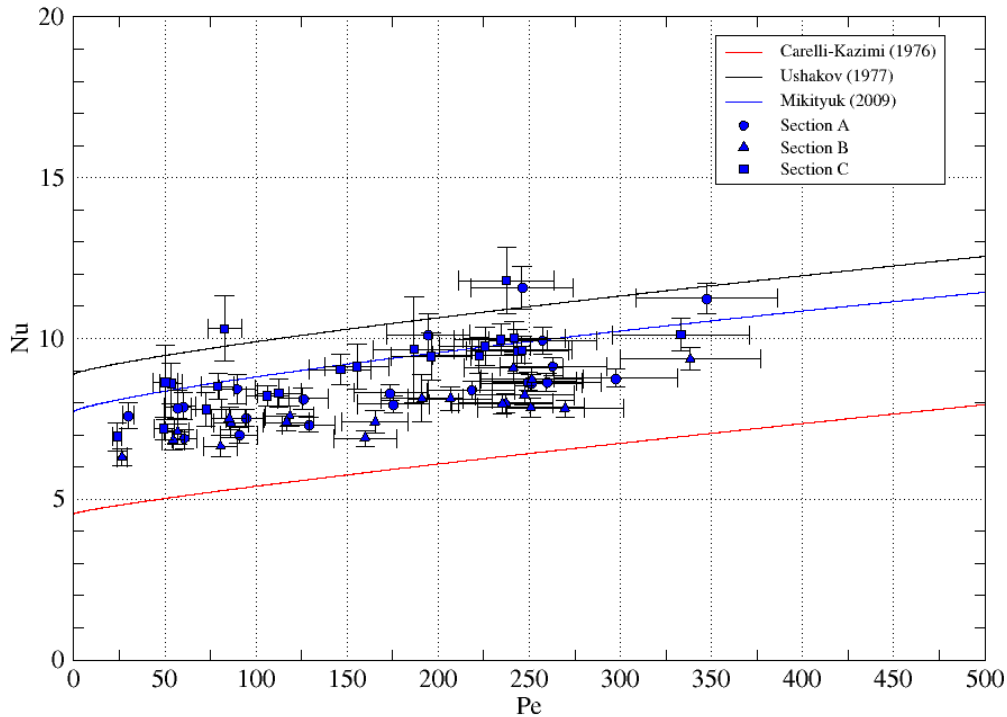
Nu 2

Figure.29: Section-averaged Nusselt number Nu₂ at all the sections for all test cases.

The same data on the heat transfer for the overall section are reported form ***Figure.30*** to ***Figure.32***, one for each monitored section. It allows to understand the general trend for the Nusselt number, as a function of the axial position. For each section, Nu_1 is lower than Nu_2. Nevertheless, the two definitions shows different behavior with increasing axial position.

Nu_1 exhibits a clear decreasing trend as the axial position increase. This behavior is a direct consequence of the fact that the difference between wall and bulk section-averaged temperatures increases with the axial position inside the active region. As analyzed in other deliverables [4] and [12], the different slope of bulk temperature and wall temperatures is the evidence that the temperature field is not yet fully developed in the whole active region (L_{active} = 600 *mm*). This behavior was already pointed out in previous work on CFD analysis on the rod bundle behavior for the experiments at the NACIE-UP facility.

As it regards the local heat transfer, discussed in previous paragraph, the same decreasing trend is shown by the subchannels S22 and S26. On the contrary, the central subchannels S2 and S5 present increasing Nusselt Numbers with higher axial position.

A third trend is displayed by Nu_2. In this case, the Nusselt versus Péclet decreases slightly going from section A to B, but then increases in section C. The same behavior is exhibited by the local Nusselt in subchannel S33.It is clear that this similarity between Nu_2 and S33 depends on the definition of Nu_2 and the significant weighting factor associated to S33 (see ***Table.6***).

An important general remark is that comparison of experimental data with correlations is a good practice to investigate the global coherence of the data set, but the specific geometry in the specific flow rate range with heavy liquid metal probably was never investigated experimentally. Therefore,

experimental data must be taken as *the reference*, and, provided the correctness of measurement methods and techniques, eventually correlations should be derived from the data.

Moreover, correlations for complex geometries (like fuel pin bundles) are generally based on largely non-uniform experimental data sets. This non-uniformity is: on the fluid (Sodium, Galistan, lead, etc..), on the geometry (wire vs. grid), on the experimental setup conditions, on the experimental measurement techniques, and on the definitions adopted for the heat transfer coefficient and Nusselt number. It was clearly shown that with the same data set, differences of 20-30% can be obtained by only changing the Nusselt averaging definitions. From this remark, probably the best practice is simply to declare very accurately the experimental setup and definitions adopted and to be very careful in comparison with correlations or other experimental data sets.

Average Nusselt numbers in the sections A, B, C, for the different cases are reported in table format in **Annex B**. Local values are reported in the same Annex.
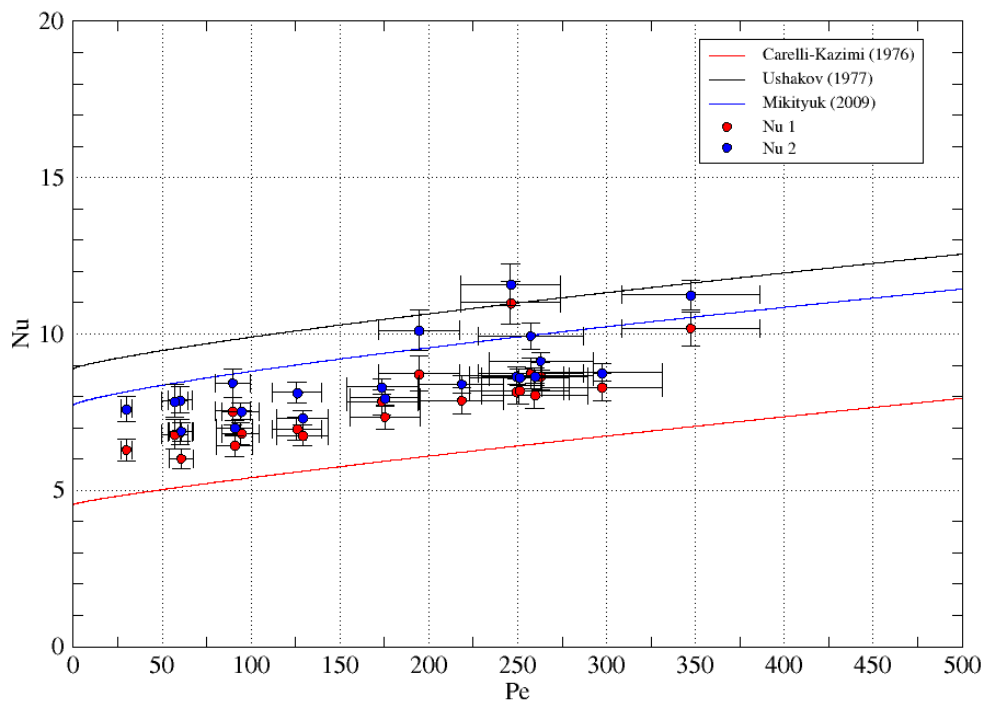

Figure.30: Section-averaged Nusselt number Nu_1 and Nu_2 at section A for all test cases.
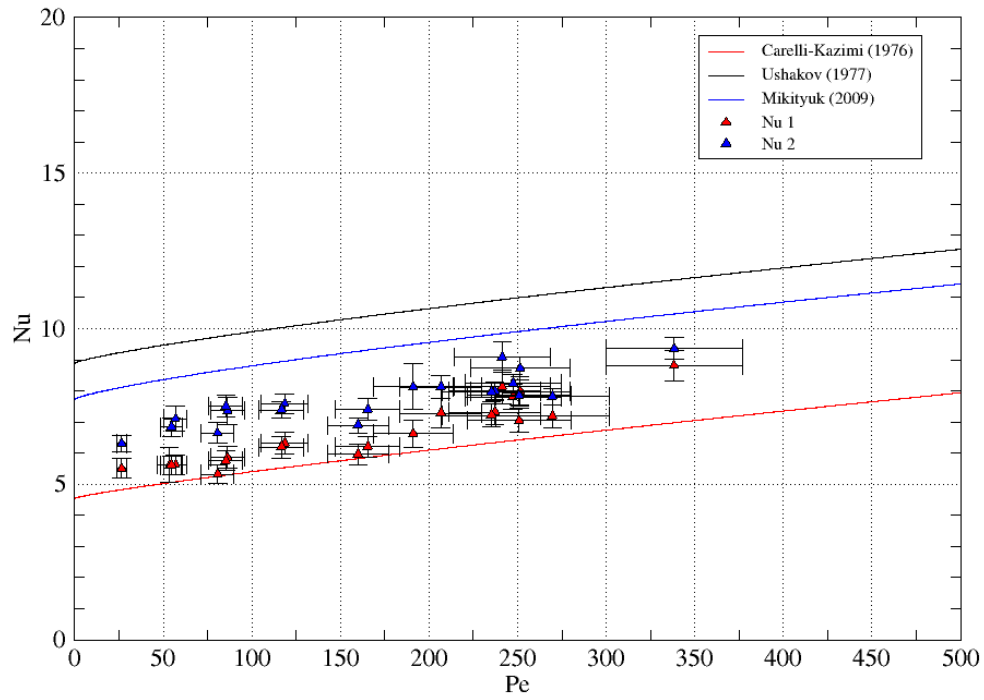
Section B

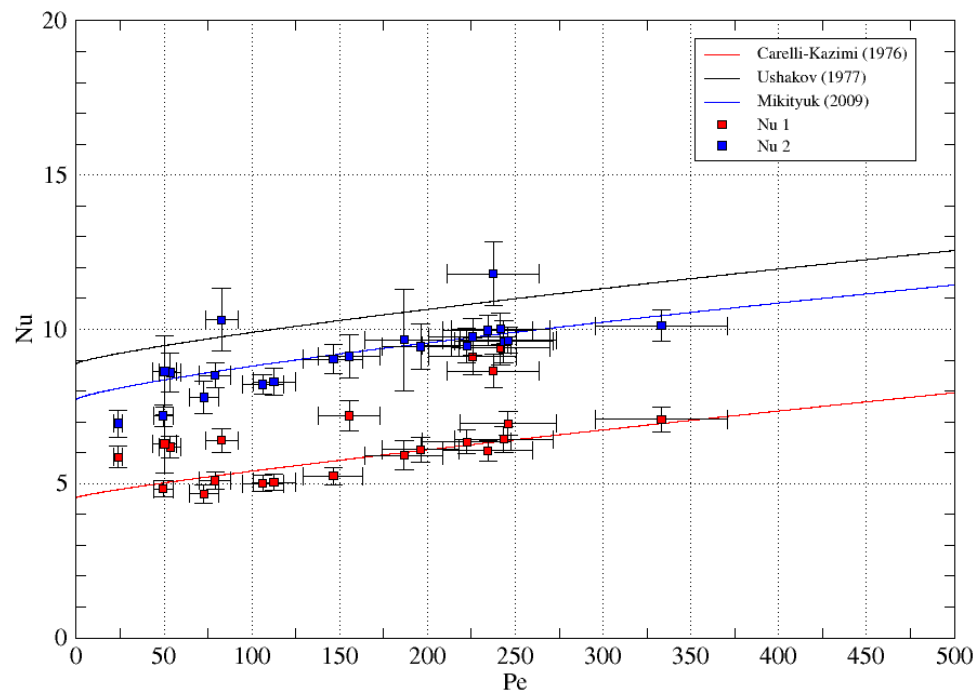***Figure.31: Section-averaged Nusselt number Nu₁ and Nu₂ at section B for all test cases.***

Section C

Figure.32: Section-averaged Nusselt number Nu₁ and Nu₂ at section C for all test cases.

o **Coolability of the MYRRHA fuel assembly**

The main objective of the experimental campaign was to assess the coolability of the MYRRHA fuel assembly during a Loss of Flow Accident (LOFA) with the coast-down of the main circulation pump. Heat transfer during a LOFA is driven by the inertia of the fluid during the pump coast-down and the onset of natural circulation due to the difference in height between the heat source and the heat sink.

For this reason, several test at different power level were performed with FPS test section placed inside the NACIE-UP facility. For each power level, different mass flow rate were tested. The aim was to evaluate the range of power and mass flow rate feasible without exceeding the clad temperature limits.

The experimental test matrix referred to power and mass flow rate conditions related to LOFA conditions in the MYRRHA fuel assembly. However, scaling factors allow to switch from MYRRHA to NACIE conditions, keeping the same subchannel velocity u_{sc} [m/s] and the same linear power density Q_{lin} [kW/m] in both the facilities.

Figure.33 shows the axial trend of clad temperature for pin 3, which is monitored in 13 axial positions. Experimental data refer to test at 11 kW of nominal power and different mass flow rates. All the cases were referred to the same temperature at the first monitored position. As the mass flow rate decreases the temperature difference between the first and the last monitored positions increase. The lowest mass flow rate performed lead to temperature increase of almost 200 °C. Lower mass flow rates would have led to higher clad temperature, also beyond the safety limits.

Power 11 kW
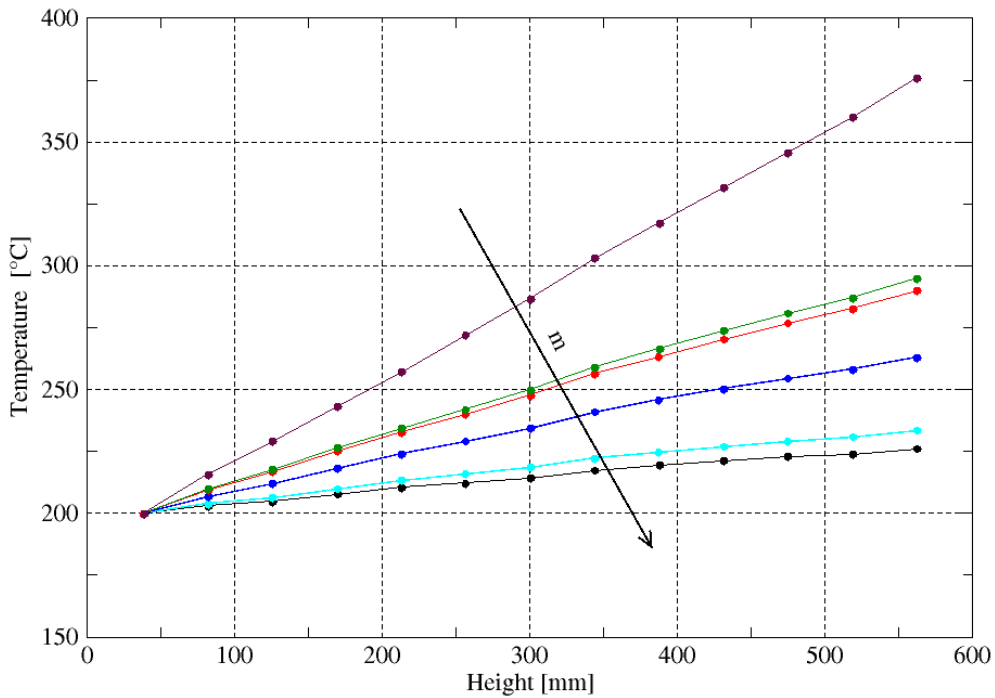
Figure.33: Wall temperature in pin 3 at different mass flow rates.

Figure.*34* shows the maximum clad temperature for each test performed in the NACIE-UP facility. The experimental data are reported as function of the mass flow rate and the power level. This graph can help to identify the range of operability of the facility for the very low mass flow rate range. For a set power level, it is possible to estimate the lowest mass flow rate achievable without exceeding the temperature limits. Decreasing the power level, it will be possible to reach lower mass flow rate in safe conditions. *Figure.35* shows the same data set of *Figure.34* but scaled to the mass flow rate and power of the MYRRHA fuel assembly.
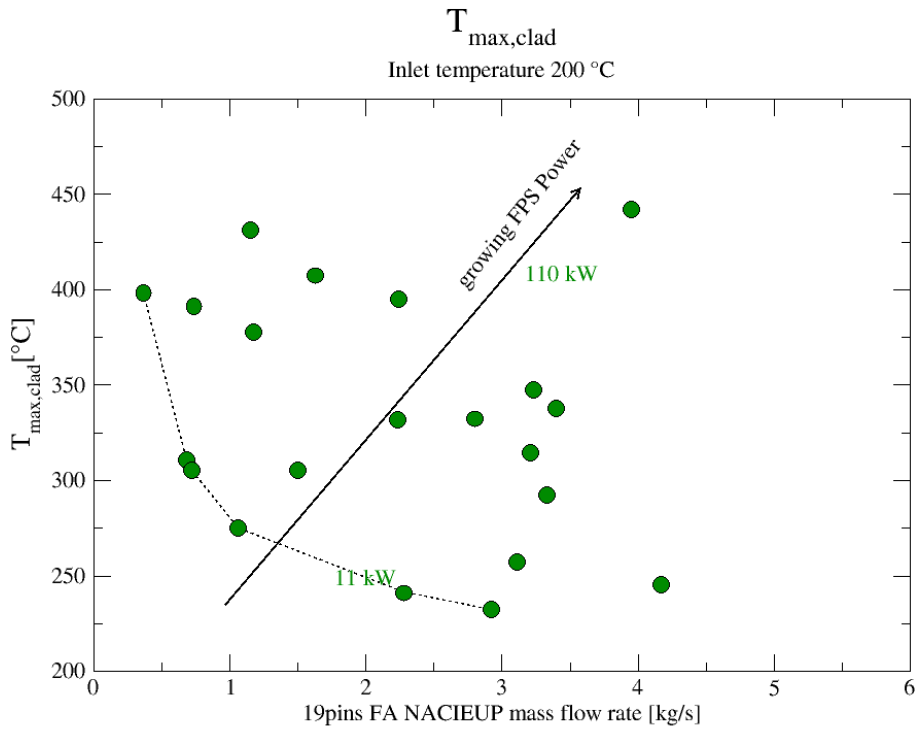
Figure.34:Maximum clad temperature achieved in the NACIE-UP facility for each test case.
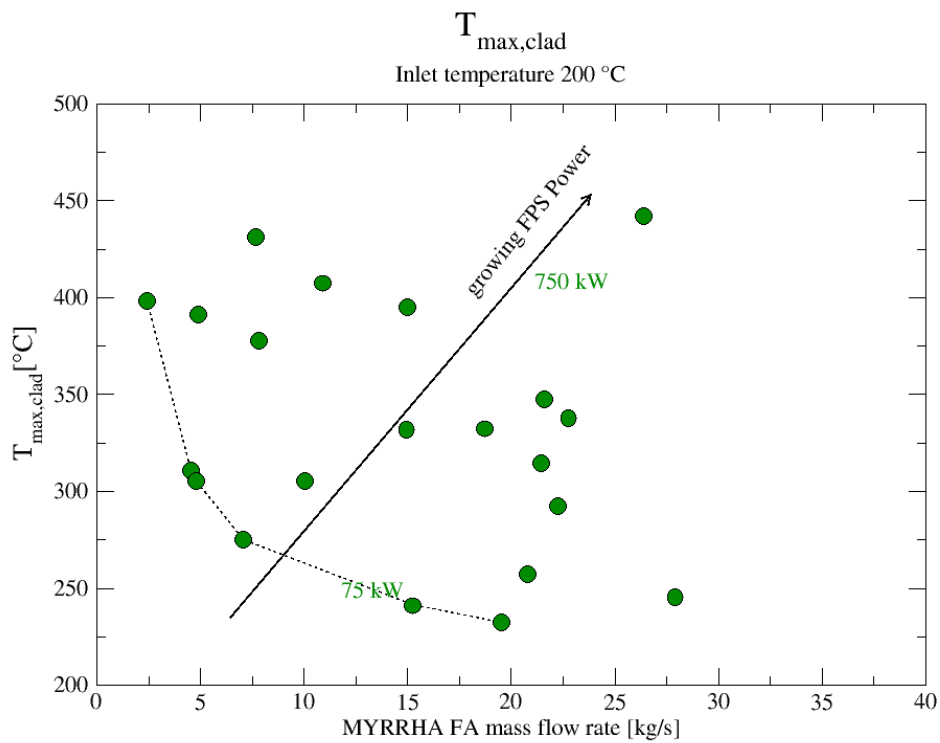
Figure.35:Maximum clad temperature scaled for the MYRRHA fuel assembly for experimental test performed with NACIE-UP facility.

- **CONCLUSIONS**

In this work, the NACIE-UP facility, located at ENEA Brasimone Research Centre, is described. The components, the instrumentation and the Data Acquisition & Control System are characterized in detail. A test section was appropriately designed and manufactured in order to perform experiments for thermal-hydraulic studies of a wire-spaced fuel pin bundle. It consists of 19 electrical pins with diameter D = 6.55 mm and active length L_{active} = 600 $mm.$ The pins are placed on an hexagonal lattice by a suitable wrapper, while spacer grids will be avoided thanks to the wire spacer.

The experimental campaign performed at ENEA with the NACIE-UP facility followed the experimental test matrix range provided by SCK-CEN. Nevertheless, the original experimental test matrix was a bit modified and adapted to the features of the facility. In particular, the main thermal-hydraulic parameters of NACIE were set in order to have analogous behavior of the MYRRHA bundle. The reference quantities for each test are: the average subchannel velocity u_{sc} [m/s], which characterize the flow from an hydraulic point of view, and the average linear power in a single pin Q_{lin} [kW/m], which defines the heat transfer boundary conditions. The subchannel velocity u_{sc} determines, on the base of the geometry of the bundle and on the fluid properties, the LBE mass flow rate in the MYRRHA FA $\dot{m}_{FA}$ [kg/s], and the LBE mass flow rate in the NACIE-UP bundle $\dot{m}_{NACIE}$ [kg/s]. Instead, the linear power density Q_{lin} [kW/m] fixes the total power of the NACIE-UP 19-pin bundle Q [kW]. The range investigated was $\dot{m}_{NACIE} \approx 0.3 - 4.2 \ kg/s$, $\dot{m}_{FA} \approx 2 - 24 \ kg/s$, $Q_{lin} \approx 1 - 10 \ kW/m$, $Q \approx 10 - 110 \ kW$. The subchannel Reynolds and Peclet numbers were respectively <12000 and <400, in the laminar or early transition range.

In this document, detailed results on heat transfer characteristics and overall coolability of the wire spaced fuel assembly for the entire experimental campaign are described. Detailed analyses of few experimental tests in natural circulation flow are reported in [12] and some cases in forced circulation regime flow are analyzed in [4].

In each experimental test, data acquisition started after that steady state conditions were reached and data collection lasted about 15-20 minutes (900-1200 samples) in order to have a set of data statistically significant.

Collected data were post-processed with a Matlab routine. The post-processing method is fully described in Section ▨. Some derived quantities are computed from measured data. All the variables adopted in the analysis were defined in Section ▨o. The OECD/NEA Handbook on Lead bismuth Eutectic Alloy Properties [11] was used as reference for the LBE properties necessary for the post-processing calculation. The error analysis method implemented is presented in Section ▨o. The chosen method allow to compute the average values of the derived quantities and their standard deviations consistently with the error propagation theory.

Then, comprehensive analysis on the heat transfer phenomena inside the FPS is presented. This study is mainly achieved through the analysis of the Nusselt number, graphically reported as a function of the Péclet number. This representation allows the comparison of the experimental data with the correlations existing in literature. Among them, three were chosen for comparison.

Two different analyses for heat transfer were performed: local ones in single subchannel and overall section analyses.

Results on local analyses generally show consistency. Nusselt number in central channels are well represented by two of the correlation chosen. Nusselt in peripheral subchannels are lower but the thermal field is affected by the heat transfer to the outer structures.

Section-averaged analysis on heat transfer showed some differences which depend on the definition adopted for the average Nusselt. In this work, two definition were chosen. The first (Nu_1) is based on section-averaged temperatures. The second one (Nu_2) is based on the weighted average among the local Nusselt numbers. The second method shows higher values of Nusselt than the first at the same Péclet. However, the first definition shows some consistencies as it regards the axial trend of Nusselt. As the axial position increases, the wall-bulk temperature difference increases and the Nusselt number decreases.

Results show in general values in between Carelli and Ushakov correlations, with Nu_1 values closer Carelli and Nu_2 values closer to Ushakov.

An important general remark is that comparison of experimental data with correlations is a good practice to investigate the global coherence of the data set, but the specific geometry in the specific flow rate range with heavy liquid metal probably was never investigated experimentally. Therefore, experimental data must be taken as *the reference*, and, provided the correctness of measurement methods and techniques, eventually correlations should be derived from the data.

Moreover, correlations for complex geometries (like fuel pin bundles) are generally based on largely non-uniform experimental data sets. This non-uniformity is: on the fluid (Sodium, Galistan, lead, etc..), on the geometry (wire vs. grid), on the experimental setup conditions, on the experimental measurement techniques, and on the definitions adopted for the heat transfer coefficient and Nusselt number. It was clearly shown that with the same data set, differences of 20-30% can be obtained by only changing the Nusselt averaging definitions. From this remark, probably the best practice is simply to declare very accurately the experimental setup and definitions adopted and to be very careful in comparison with correlations or other experimental data sets.

Finally, some considerations on the overall coolability of the MYRRHA fuel assembly are deduced. The maximum clad temperature graphs can help to identify the range of operability of the MYRRHA fuel assembly for the very low mass flow rate range. It allows to estimate the lowest mass flow rate achievable without exceeding the temperature limits, once the power level is set.

Although some results were obtained, future developments are foreseen. The experimental matrix need to be completed and the full range of power and mass flow rate needs to be investigated.

Further, both the fulfillment of the experiments and the equipment of the facility can be improved in instrumentation and operational conditions. The restoration and calibration of the induction flow meter (FM102) is already fulfilled. A new mass flow meter, specifically intended to measure with accuracy lower mass flow rates is under manufacture. Also, differential pressure transducers will be installed on the test section for a more accurate measurement of the pressure losses across the fuel pin bundle simulator and to better measure the pressure head provided by the gas injection system.

NOMENCLATURE

Roman letters

A	Pipe area
a	Apothem of the hexagonal wrap
c_p	Specific heat
D	Pin diameter
D_{eq}	Equivalent diameter of the subchannel
D_h	Hydraulic diameter
d	Wire diameter
d_t	Tube diameter
F	Geometrical parameter for friction factor
f	Darcy-Weisbach friction coefficient
g	Gravity acceleration
Gr	Grashof number
Gr_t	Transversal Grashof number
H	Difference in height between heat source and heat sink
H_{riser}	Height of the riser
h	Heat transfer coefficient
K	Resistance coefficient
K_{conc}	Singular resistance coefficient
k	Fluid conductivity
L_{active}	Active length of the pin
L_{bundle}	Wire-spaced bundle length
L_{total}	Total length of the pin
L_w	*W*etted parameter
l	Side length of the hexagonal wrap
M	Number of pins
$\dot{m}$	Mass flow rate
N	Number of pin rank
Nu	Nusselt number
P	Bundle pitch
P_w	Wire pitch
Pe	Péclet number
Q	Bundle total power
Q_{lin}	Linear power
Q_{nom}	Nominal power
q''	Wall heat flux
Re	Reynolds number
Ri_t	Transversal Richardson number
S_t	Total wetted perimeter
T_{ac}	Acquired Temperature

T_b	Bulk Temperature
T_{clad}	Cladding Temperature
T_w	Wall Temperature
u	Velocity
v_{bv}	Brunt-Vaisala velocity
z	Vertical coordinate from the beginning of the active region

Greek Letters

α	Gas void fraction
β	Thermal expansion coefficient
δ	Nominal gap between wire and pin
Δp_{loss}	Overall pressure losses
ΔT	Axial temperature drop
ΔT_t	Transversal temperature drop
ϑ	Azimuthal angle of the pin
ρ	Fluid density
ν	Cinematic viscosity

Abbreviations and acronyms

CFD	Computational Fluid Dynamics
DACS	Data Acquisition and Control System
FPS	Fuel Pin bundle Simulator
HTC	Heat Transfer Coefficient
HX	Heat Exchanger
I.D.	Internal Diameter
LBE	Lead-Bismuth Eutectic
LOFA	LOss of Flow Accident
P&ID	Piping and Instrumentation Diagram
TC	Thermocouple
TC-FPS-XX	Conventional name of thermocouples

Subscript

bundle	Refers to the bundle
pins	Refers to pins
sc	Refers to subchannels
tubes	Refers to the main pipe
wire	Refers to wires around the pins
wrap	Refers to hexagonal wrap of the bundle

REFERENCES

[1] H.A. Abderrahima, P. Kupschusa, E. Malambua, Ph. Benoita, K. Van Tichelen, B. Ariena, F. Vermeerscha, P. D'hondta, Y. Jongenb, S. Ternierb, D. Vandeplassche, MYRRHA: A multipurpose accelerator driven system for research & development, *Nuclear Instruments and Methods in Physics Research* A, vol. 463, pp. 487-494, 2001.

[2] M. Scarpa, CFD Thermal Hydraulic Analysis of HLM cooled rod bundles, Master Thesis Univ. of Pisa, Italy, 2013.

[3] I. Di Piazza, M. Tarantino, P. Gaggini, Main Process for the Logical Control of the NACIE-UP loop, NA-I-M-0003 ENEA C.R. Brasimone Report, 2013.

[4] AA.VV. Deliverable D-N° 2. 6, Experimental results on forced convection in heavy liquid metals using the NACIE facility

[5] I. Di Piazza, D. Martelli, Experimental Circulation Tests on a prototypical inductive flow meter with the NACIE loop, NA-T-R-029 ENEA C.R. Brasimone Report, 2013.

[6] AA.VV. Deliverable D-N° 2.3, NACIE: a test facility for free and mixed convection heat transfer measurements in liquid metals for the MYRRHA reactor.

[7] K. Van Tickelen, private communication, 2014.

[8] http://www.ni.com/labview/

[9] S. Keijers, Measurement range for the heat transfer correlation in the wire spacer rod bundle of MYRRHA, SCK•CEN-R-5327, 2012.

[10] D. LeCharpentier, Thermocoax, private communication, 2015.

[11] OECD/NEA Nuclear Science Committee, Handbook on Lead bismuth Eutectic Alloy and Lead Properties, Materials Compatibility, Thermal-hydraulics and Technologies, 2007 Edition.

[12] AA.VV. Deliverable D-N° 2. 4, Experimental results on free convection in heavy liquid metals using the NACIE facility.

[13] W.Pfrang, D.Struwe, Assessment of Correlations for Heat Transfer to the Coolant for Heavy Liquid Metal Cooled Core Design, *Institut für Reaktorsicherheit*, Karlsruhe, 2007.

[14] K. Mikityuk, Heat transfer to liquid metal: Review of data and correlation for tube bundles, *Nuclear Engineering and Design,* vol. 239, pp. 680-687, 2009.

[15] R. Marinari, Pre-Test analysis of the rod bundle experiment in the Heavy Liquid Metal facility NACIE-UP, Master Thesis University of Pisa, Italy, 2014.

- **Annex A**

```
% POST-PROCESSING Experimental data from NACIE-UP FPS-19250 experiments
% Experiments in statistically steady state condition
% Each data set corresponds to a single test of the test matrix (es. P220)
clear all;close all;clc;
% Open File Experimental DATA
Ainput = dlmread( 'P269.txt','\t',1,2);
[n, m] = size (Ainput);
%
% Write output file
fileIDO = fopen('POST_NACIE_rev6.dat','a+');
formatO= '%10.4g \t';
formatOh = '%10s \t';
%
%-------------------------------%
% Geometrical DATA of the bundle  %
%-------------------------------%
Npin = 19;
Dpin = 6.55e-3;  % pin diameter [m]
Dwire = 1.75e-3; % wire diameter [m]
p = 8.4e-3;      % lattice pitch [m]
delta = 0.1e-3;  % distance between wire and adiacent pin [m]
a = sqrt(3)/2. * p *2.+ Dpin /2. + Dwire + delta; %apothem of hexagonal wrapper internal wall
[m]
l = 2. / sqrt(3) * a; % side of hexagonal wrapper internal wall [m]
L_ac = 0.6;       % Active length [m]
Area = (3 *l^2 * sqrt(3)/2)- Npin * pi/4* (Dpin^2 + Dwire^2); % Area fuel bundle
D_h = 3.836e-3;    % Hydraulic diameter of the infinite lattice bundle [m]
%-------------------------------%
% ISTRUMENTS data and deviation  %
%-------------------------------%
TCb_std = 0.1; % standard deviation error of FPS TC [K]
TCl_std = 1.; % standard deviation error of loop TC [K]
fr = 1.;       % sampling frequency [Hz]
Q_std = 0.1;  % standard deviation  error power [W]
FM101_std = 0.1; % standard deviation error LBE mass flow rate [kg/s]
P_std = 0.01; % standard deviation error of the pressure measure bubble tube [bar]
%
% vector time created from sampling frequency fr
deltat = 1. / fr; %time interval between samplings
tmax = (n-1)*deltat;
time = [0.:deltat:tmax];
time =time';
%--------------------------%
%     POWER and HEAT FLUX    %
%--------------------------%
% disp('Insert total FPS power in kW ');
% Pow = input('Q [kW] = ');
% Pow = Pow * 1000.;
% Q = Pow + normrnd(0,Q_std,n,1);
% Q_av = mean(Q);
% Q_std = std(Q);
Q = 0.97*1000*Ainput(:,7); % to read power from measurement
Q = Q + normrnd(0,Q_std,n,1);
Q_av = mean(Q);
Q_std = std(Q);
q_s = Q ./ (Npin * L_ac * pi * Dpin); %heat flux vector[W/m^2]
q_lin = Q / Npin / L_ac;
%-----------------------------------------------------%
%       Regressione lineare temperature primario      %
%-----------------------------------------------------%
%procedura per eliminare dai dati l'andamento crescente nel tempo
%(circa leneare) e riportare a condizione stazionario con temperatura
%media costante nel tempo
% pol = polyfit(time, Ainput(:,66),1);
% retta = - pol(1,1) .* time + n/2 * pol(1,1);
% for i = 1:m
```

```
%      Ainput(:,i)=Ainput(:,i) - retta;
% end
%-------------------------------------------------------%
% TC-LBE loop temperatures vectors and average values  %
%-------------------------------------------------------%
TP101 = [Ainput(:,132)]; %LBE temperature at FPS inlet
TP101 = TP101 + normrnd(0,TCl_std,n,1);
TP102 = [Ainput(:,133)]; %LBE temperature at FPS outlet
TP102 = TP102 + normrnd(0,TCl_std,n,1);
TP103 = [Ainput(:,134)]; %hot LBE temperature mixed
TP103 = TP103 + normrnd(0,TCl_std,n,1);
TP104 = [Ainput(:,135)]; %hot LBE temperature mixed
TP104 = TP104 + normrnd(0,TCl_std,n,1);
TP105 = [Ainput(:,136)]; %hot LBE temperature mixed
TP105 = TP105 + normrnd(0,TCl_std,n,1);
TP106 = [Ainput(:,137)]; %hot LBE temperature mixed
TP106 = TP106 + normrnd(0,TCl_std,n,1);
TP107 = [Ainput(:,139)]; %hot LBE temperature mixed
TP107 = TP107 + normrnd(0,TCl_std,n,1);
TFM101= [Ainput(:,131)]; %hot LBE temperature mixed
TFM101 = TFM101 + normrnd(0,TCl_std,n,1);
%---------------------------%
%    PRESSURE MEASUREMENTS   %
%---------------------------%
P101 = [Ainput(:,32)];
P101 = P101 + normrnd(0,P_std,n,1);
P102 = [Ainput(:,33)];
P102 = P102 + normrnd(0,P_std,n,1);
P103 = [Ainput(:,34)];
P103 = P103 + normrnd(0,P_std,n,1);
P104 = [Ainput(:,35)];
P104 = P104 + normrnd(0,P_std,n,1);
P105 = [Ainput(:,36)];
P105 = P105 + normrnd(0,P_std,n,1);
P110 = [Ainput(:,37)];
P110 = P110 + normrnd(0,P_std,n,1);
H1_2 = 1.5635; %[m]
H3_5 = 4.6905; %[m]
FPS_avg = 0.5 .* (TP101+TP103);
[~, ~, LBE_rho1_2, ~] = LBE(FPS_avg+273.15);
[~, ~, LBE_rho3_5, ~] = LBE(TP104+273.15);
LBE_rho1_2 = LBE_rho1_2 + normrnd(0,0.8 ./100.* LBE_rho1_2,n,1);
LBE_rho3_5 = LBE_rho3_5 + normrnd(0,0.8 ./100.* LBE_rho3_5,n,1);
batt1_2 = LBE_rho3_5 .* 9.81 .* H1_2 .* 1.e-05;
batt3_5 = LBE_rho1_2 * 9.81 * H3_5 .* 1.e-05;
DP_FPS = P101-P102-batt1_2;
DP_head = batt3_5-(P103-P105);
%-------------------------------------------------------%
% TC-FPS temperatures vectors and average values  %
%-------------------------------------------------------%
% TC_FPS: 67 column matrix with TC_FPS_01 to TC_FPS_67 values
% TC_FPSo: 3 column matrix with TC_FPS_108 to TC_FPS_110 values
% TC_FPS_e 67 column matrix with TC_FPS_01 to TC_FPS_67 values with random
% errors
% TC_FPS_av one row 67 column matrix with avg values for TC_FPS 01 to 67
% TC_FPS_std one row 67 column matrix with std values for TC_FPS 01 to 67
% analogous for TC_FPS 108 to 110
TC_FPS = [Ainput(:, 61:70) Ainput(:, 73) Ainput(:, 75:130)];
TC_FPSo = [Ainput(:, 71) Ainput(:, 72) Ainput(:, 74)];
%
TC_FPS_e = [];
TC_FPS_av = [];
TC_FPS_std = [];
TC_FPSo_e = [];
TC_FPSo_av = [];
TC_FPSo_std = [];

for i = 1:67
    nextcole = TC_FPS(:,i) + normrnd(0,TCb_std,n,1);
    nextcolav = mean(nextcole);
    nextcolstd = std(nextcole);
    TC_FPS_e = [TC_FPS_e nextcole];
    TC_FPS_av = [TC_FPS_av; nextcolav];
    TC_FPS_std = [TC_FPS_std; nextcolstd];
end
```

```
for i = 1:3
    nextcole = TC_FPSo(:,i) + normrnd(0,TCb_std,n,1);
    nextcolav = mean(nextcole);
    nextcolstd = std(nextcole);
    TC_FPSo_e = [TC_FPSo_e nextcole];
    TC_FPSo_av = [TC_FPSo_av nextcolav];
    TC_FPSo_std = [TC_FPSo_std nextcolstd];
end
%-------------------------------------------------------%
% Correction for Wall embedded thermocouple position   %
%-------------------------------------------------------%
TC_FPS_w = [];
TC_FPS_w_av = [];
TC_FPS_w_std = [];
% TC_FPS_w is 67 columns matrix
% From columns 1 to 15 TC_FPS_w = TC_FPS_e (bulk temperatures )
% From columns 16 to 67 contains with extrapolated wall temperature
% These values are used to compute Nusselt number
for i = 1:15
    TC_FPS_w(:,i) =  TC_FPS_e(:,i);
    TC_FPS_w_av(:,i) = mean(TC_FPS_w(:,i));
    TC_FPS_w_std(:,i) = std(TC_FPS_w(:,i));
end
for i = 16:67 % TC FPS 1 to 15 are bulk TCs
    k_ss =AISI304L(TC_FPS_e(:,i));
        TC_FPS_w(:,i) =  TC_FPS(:,i) - q_lin ./ (2. * pi * k_ss)*...
        log((Dpin/2)/(Dpin/2-0.00035/2));
    TC_FPS_w_av(:,i) = mean(TC_FPS_w(:,i));
    TC_FPS_w_std(:,i) = std(TC_FPS_w(:,i));
end
%-------------------------------------------------------%
%       FPS  Tinlet & Toulet extrapolation            %
%-------------------------------------------------------%
% FPS inlet & outlet temperature are extrapolated from
% the measured bulk temperature weighted on the subchannel areas
w2  = 0.058;
w5  = 0.058;
w22 = 0.346;
w26 = 0.179;
w33 = 0.359;
TbulkA =  TC_FPS_e(:, 1).* w2 + TC_FPS_e(:, 2).* w5 + TC_FPS_e(:, 3).* w22 +...
    TC_FPS_e(:, 4).*w26 + TC_FPS_e(:, 5).*w33;
TbulkB =  TC_FPS_e(:, 6).* w2 + TC_FPS_e(:, 7).* w5 + TC_FPS_e(:, 8).*w22 +...
    TC_FPS_e(:, 9).*w26 + TC_FPS_e(:, 10).*w33;
TbulkC =  + TC_FPS_e(:,12).* (w5+w2) + TC_FPS_e(:, 13).*w22 +...
    TC_FPS_e(:, 14).*w26 + TC_FPS_e(:, 15).*w33;
TbulkA_av  = mean(TbulkA);
TbulkA_std = std(TbulkA);
TbulkB_av  = mean(TbulkB);
TbulkB_std = std(TbulkB);
TbulkC_av  = mean(TbulkC);
TbulkC_std = std(TbulkC);
Tinlet = TbulkA - ((TbulkC - TbulkA)/(262*2)*38);
Toutlet = TbulkC + ((TbulkC - TbulkA)/(262*2)*38);
Tinlet_av  = mean(Tinlet)
Tinlet_std  = std(Tinlet);
Toutlet_av  = mean(Toutlet)
Toutlet_std = std(Toutlet);
%---------------------------%
%       MASS FLOW RATE      %
%---------------------------%
% Mf = [Ainput(:,3)]; %mass flow rate from FM101
% Mf = Mf + normrnd(0,FM101_std,n,1);
% [cpI, ~, ~, ~] = LBE(Tinlet+273.15);
% cpI = cpI + normrnd(0,1./100.*cpI,n,1);
% [cpO, ~, ~, ~] = LBE(Toutlet+273.15);
% cpO = cpO + normrnd(0,1./100.*cpO,n,1);
% Mf = Q ./ [cpO .*(Toutlet+273.15) - cpI .*(Tinlet+273.15)];
FPS_avg = 0.5 .* (Tinlet+Toutlet);
[cpFPS, ~, ~, ~] = LBE(FPS_avg+273.15);
cpFPS = cpFPS + normrnd(0,7./100.*cpFPS,n,1);
Mf = Q ./ (cpFPS .*(Toutlet-Tinlet));
Mf_av = mean(Mf)
Mf_std = std(Mf);
```

```
%--------Derived variables---------%
%--------------------------------%
%            SECTION A            %
%--------------------------------%
%----Re and Pr on the section A----%
% Tb_avA = (TC_FPS_e(:,1) + TC_FPS_e(:,2) + TC_FPS_e(:,3)+...
%     TC_FPS_e(:,4)+ TC_FPS_e(:,5))./5.;
[LBE_cp, LBE_cond, ~, LBE_mi] = LBE(TbulkA+273.15);
LBE_cp = LBE_cp + normrnd(0,7./100.*LBE_cp,n,1);
LBE_cond = LBE_cond + normrnd(0,5./100.*LBE_cond,n,1);
LBE_mi = LBE_mi + normrnd(0,5./100.*LBE_mi,n,1);
Re_A = Mf ./ Area .* D_h ./ LBE_mi;
Re_A_av = mean(Re_A);
Re_A_std = std(Re_A);
Pr_A = LBE_mi .* LBE_cp ./ LBE_cond;
Pr_A_av = mean(Pr_A);
Pr_A_std = std(Pr_A);
Pe_A = Re_A .* Pr_A;
Pe_A_av = mean(Pe_A);
Pe_A_std = std(Pe_A);
%---------Subchannel S2-----------%
Tw_S2A = (TC_FPS_w(:, 16) + TC_FPS_w(:, 18) + TC_FPS_w(:, 24))./3.;
Tw_S2A_av = mean(Tw_S2A);
Tw_S2A_std = std(Tw_S2A);
Tb_S2A = TC_FPS_e(:, 1);
Tb_S2A_av = mean(Tb_S2A);
Tb_S2A_std = std(Tb_S2A);
HTC_S2A = q_s ./ (Tw_S2A-Tb_S2A);
HTC_S2A_av = mean(HTC_S2A);
HTC_S2A_std = std(HTC_S2A);
[~, LBE_cond, ~, ~] = LBE(Tb_S2A+273.15); % vettori prop
LBE_cond = LBE_cond + normrnd(0,5./100.*LBE_cond,n,1);
Nu_S2A = HTC_S2A .* D_h ./ LBE_cond;
Nu_S2A_av = mean(Nu_S2A);
Nu_S2A_std = std(Nu_S2A);
%---------- Subchannel 5 ----------%
Tw_S5A = (TC_FPS_w(:, 17) + TC_FPS_w(:, 19) + TC_FPS_w(:, 20))./3.;
Tw_S5A_av = mean(Tw_S5A);
Tw_S5A_std = std(Tw_S5A);
Tb_S5A = TC_FPS_e(:, 2);
Tb_S5A_av = mean(Tb_S5A);
Tb_S5A_std = std(Tb_S5A);
HTC_S5A = q_s ./ (Tw_S5A-Tb_S5A);
HTC_S5A_av = mean(HTC_S5A);
HTC_S5A_std = std(HTC_S5A);
[~, LBE_cond, ~, ~] = LBE(Tb_S5A+273.15); % vettori prop
LBE_cond = LBE_cond + normrnd(0,5./100.*LBE_cond,n,1);
Nu_S5A = HTC_S5A .* D_h ./ LBE_cond;
Nu_S5A_av = mean(Nu_S5A);
Nu_S5A_std = std(Nu_S5A);
%---------- Subchannel 22 ----------%
Tw_S22A = (TC_FPS_w(:, 21) + TC_FPS_w(:, 23) + TC_FPS_w(:, 26))./3.;
Tw_S22A_av = mean(Tw_S22A);
Tw_S22A_std = std(Tw_S22A);
Tb_S22A = TC_FPS_e(:, 3);
Tb_S22A_av = mean(Tb_S22A);
Tb_S22A_std = std(Tb_S22A);
HTC_S22A = q_s ./ (Tw_S22A-Tb_S22A);
HTC_S22A_av = mean(HTC_S22A);
HTC_S22A_std = std(HTC_S22A);
[~, LBE_cond, ~, ~] = LBE(Tb_S22A+273.15); % vettori prop
LBE_cond = LBE_cond + normrnd(0,5./100.*LBE_cond,n,1);
Nu_S22A = HTC_S22A .* D_h ./ LBE_cond;
Nu_S22A_av = mean(Nu_S22A);
Nu_S22A_std = std(Nu_S22A);
%---------- Subchannel 26 ----------%
Tw_S26A = (TC_FPS_w(:, 27) + TC_FPS_w(:, 28))./2.;
Tw_S26A_av = mean(Tw_S26A);
Tw_S26A_std = std(Tw_S26A);
Tb_S26A = TC_FPS_e(:, 4);
Tb_S26A_av = mean(Tb_S26A);
Tb_S26A_std = std(Tb_S26A);
HTC_S26A = q_s ./ (Tw_S26A-Tb_S26A);
HTC_S26A_av = mean(HTC_S26A);
HTC_S26A_std = std(HTC_S26A);
```

```
[~, LBE_cond, ~, ~] = LBE(Tb_S26A+273.15); % vettori prop
LBE_cond = LBE_cond + normrnd(0,5./100.*LBE_cond,n,1);
Nu_S26A = HTC_S26A .* D_h ./ LBE_cond;
Nu_S26A_av = mean(Nu_S26A);
Nu_S26A_std = std(Nu_S26A);
%---------- Subchannel 33 ----------%
Tw_S33A = TC_FPS_w(:, 25);
Tw_S33A_av = mean(Tw_S33A);
Tw_S33A_std = std(Tw_S33A);
Tb_S33A = TC_FPS_e(:, 5);
Tb_S33A_av = mean(Tb_S33A);
Tb_S33A_std = std(Tb_S33A);
HTC_S33A = q_s ./ (Tw_S33A-Tb_S33A);
HTC_S33A_av = mean(HTC_S33A);
HTC_S33A_std = std(HTC_S33A);
[~, LBE_cond, ~, ~] = LBE(Tb_S33A+273.15); % vettori prop
LBE_cond = LBE_cond + normrnd(0,5./100.*LBE_cond,n,1);
Nu_S33A = HTC_S33A .* D_h ./ LBE_cond;
Nu_S33A_av = mean(Nu_S33A);
Nu_S33A_std = std(Nu_S33A);
%----------------------------%
%      Average Nu in section A    %
%----------------------------%
TwallA = Tw_S2A .* w2 + Tw_S5A .* w5 + Tw_S22A .* w22+...
    Tw_S26A .* w26 + Tw_S33A .* w33;
TwallA_av = mean (TwallA);
TwallA_std = std(TwallA);
HTC_A = q_s ./ (TwallA - TbulkA);
HTC_A_av = mean(HTC_A);
HTC_A_std = std(HTC_A);
[~, LBE_cond, ~, ~] = LBE(TbulkA+273.15);
LBE_cond = LBE_cond + normrnd(0,5./100.*LBE_cond,n,1);
Nu_A = HTC_A .* D_h ./ LBE_cond;
Nu_A_av = mean(Nu_A);
Nu_A_std = std(Nu_A);
% Average Nu from weighted Subchannel Nu
Av_Nu_A = Nu_S2A .* w2 + Nu_S5A .* w5 + Nu_S22A .* w22 + ...
    Nu_S26A .* w26 + Nu_S33A .* w33;
Av_Nu_A_av = mean(Av_Nu_A);
Av_Nu_A_std = std(Av_Nu_A);
% Average Nu KIT methodology
Tw_A_kit = (Tw_S2A ./4. + Tw_S5A ./4. + Tw_S22A ./4. + Tw_S26A ./6. + Tw_S33A ./12.);
HTC_A_kit = q_s ./ (Tw_A_kit - TbulkA);
Nu_A_kit = HTC_A_kit .* D_h ./ LBE_cond;
Nu_A_kit_av  = mean(Nu_A_kit);
Nu_A_kit_std = std(Nu_A_kit);
%----------------------------%
%          SECTION B          %
%----------------------------%
%----Re and Pr on the section B----%
% Tb_avB = (TC_FPS_e(:,6) + TC_FPS_e(:,7) + TC_FPS_e(:,8)+...
%     TC_FPS_e(:,9)+ TC_FPS_e(:,10))./5.;
[LBE_cp, LBE_cond, ~, LBE_mi] = LBE(TbulkB+273.15);
LBE_cp = LBE_cp + normrnd(0,7./100.*LBE_cp,n,1);
LBE_cond = LBE_cond + normrnd(0,5./100.*LBE_cond,n,1);
LBE_mi = LBE_mi + normrnd(0,5./100.*LBE_mi,n,1);
Re_B = Mf ./ Area .* D_h ./ LBE_mi;
Re_B_av = mean(Re_B);
Re_B_std = std(Re_B);
Pr_B = LBE_mi .* LBE_cp ./ LBE_cond;
Pr_B_av = mean(Pr_B);
Pr_B_std = std(Pr_B);
Pe_B = Re_B .* Pr_B;
Pe_B_av = mean(Pe_B);
Pe_B_std = std(Pe_B);
%--------- Subchannel S2 ----------%
Tw_S2B = (TC_FPS_w(:, 29) + TC_FPS_w(:, 31) + TC_FPS_w(:, 37))/3.;
Tw_S2B_av = mean(Tw_S2B);
Tw_S2B_std = std(Tw_S2B);
Tb_S2B = TC_FPS_e(:, 6);
Tb_S2B_av = mean(Tb_S2B);
Tb_S2B_std = std(Tb_S2B);
HTC_S2B = q_s ./ (Tw_S2B-Tb_S2B);
HTC_S2B_av = mean(HTC_S2B);
HTC_S2B_std = std(HTC_S2B);
```

```
[~, LBE_cond, ~, ~] = LBE(Tb_S2B+273.15); % vettori prop
LBE_cond = LBE_cond + normrnd(0,5./100.*LBE_cond,n,1);
Nu_S2B = HTC_S2B .* D_h ./ LBE_cond;
Nu_S2B_av = mean(Nu_S2B);
Nu_S2B_std = std(Nu_S2B);
%--------- Subchannel S5 ---------%
Tw_S5B = (TC_FPS_w(:, 30) + TC_FPS_w(:, 32) + TC_FPS_w(:, 33))./3.;
Tw_S5B_av = mean(Tw_S5B);
Tw_S5B_std = std(Tw_S5B);
Tb_S5B = TC_FPS_e(:, 7);
Tb_S5B_av = mean(Tb_S5B);
Tb_S5B_std = std(Tb_S5B);
HTC_S5B = q_s ./ (Tw_S5B-Tb_S5B);
HTC_S5B_av = mean(HTC_S5B);
HTC_S5B_std = std(HTC_S5B);
[~, LBE_cond, ~, ~] = LBE(Tb_S5B+273.15); % vettori prop
LBE_cond = LBE_cond + normrnd(0,5./100.*LBE_cond,n,1);
Nu_S5B = HTC_S5B .* D_h ./ LBE_cond;
Nu_S5B_av = mean(Nu_S5B);
Nu_S5B_std = std(Nu_S5B);
%--------- Subchannel S22 ---------%
Tw_S22B = (TC_FPS_w(:, 34) + TC_FPS_w(:, 36) + TC_FPS_w(:, 39))./3.;
Tw_S22B_av = mean(Tw_S22B);
Tw_S22B_std = std(Tw_S22B);
Tb_S22B = TC_FPS_e(:, 8);
Tb_S22B_av = mean(Tb_S22B);
Tb_S22B_std = std(Tb_S22B);
HTC_S22B = q_s ./ (Tw_S22B-Tb_S22B);
HTC_S22B_av = mean(HTC_S22B);
HTC_S22B_std = std(HTC_S22B);
[~, LBE_cond, ~, ~] = LBE(Tb_S22B+273.15); % vettori prop
LBE_cond = LBE_cond + normrnd(0,5./100.*LBE_cond,n,1);
Nu_S22B = HTC_S22B .* D_h ./ LBE_cond;
Nu_S22B_av = mean(Nu_S22B);
Nu_S22B_std = std(Nu_S22B);
%--------- Subchannel S26 ---------%
Tw_S26B = (TC_FPS_w(:, 40) + TC_FPS_w(:, 41))./2.;
Tw_S26B_av = mean(Tw_S26B);
Tw_S26B_std = std(Tw_S26B);
Tb_S26B = TC_FPS_e(:, 9);
Tb_S26B_av = mean(Tb_S26B);
Tb_S26B_std = std(Tb_S26B);
HTC_S26B = q_s ./ (Tw_S26B-Tb_S26B);
HTC_S26B_av = mean(HTC_S26B);
HTC_S26B_std = std(HTC_S26B);
[~, LBE_cond, ~, ~] = LBE(Tb_S26B+273.15); % vettori prop
LBE_cond = LBE_cond + normrnd(0,5./100.*LBE_cond,n,1);
Nu_S26B = HTC_S26B .* D_h ./ LBE_cond;
Nu_S26B_av = mean(Nu_S26B);
Nu_S26B_std = std(Nu_S26B);
%--------- Subchannel S33 ---------%
Tw_S33B = TC_FPS_w(:, 38);
Tw_S33B_av = mean(Tw_S33B);
Tw_S33B_std = std(Tw_S33B);
Tb_S33B = TC_FPS_e(:, 10);
Tb_S33B_av = mean(Tb_S33B);
Tb_S33B_std = std(Tb_S33B);
HTC_S33B = q_s ./ (Tw_S33B-Tb_S33B);
HTC_S33B_av = mean(HTC_S33B);
HTC_S33B_std = std(HTC_S33B);
[~, LBE_cond, ~, ~] = LBE(Tb_S33B+273.15); % vettori prop
LBE_cond = LBE_cond + normrnd(0,5./100.*LBE_cond,n,1);
Nu_S33B = HTC_S33B .* D_h ./ LBE_cond;
Nu_S33B_av = mean(Nu_S33B);
Nu_S33B_std = std(Nu_S33B);
%-------------------------------%
%      Average Nu in section B      %
%-------------------------------%
TwallB = Tw_S2B .* w2 + Tw_S5B .* w5 + Tw_S22B .* w22+...
    Tw_S26B .* w26 + Tw_S33B .* w33;
TwallB_av = mean (TwallB);
TwallB_std = std(TwallB);
HTC_B = q_s ./ (TwallB - TbulkB);
HTC_B_av = mean(HTC_B);
HTC_B_std = std(HTC_B);
```

```
[~, LBE_cond, ~, ~] = LBE(TbulkB+273.15);
LBE_cond = LBE_cond + normrnd(0,5./100.*LBE_cond,n,1);
Nu_B = HTC_B .* D_h ./ LBE_cond;
Nu_B_av = mean(Nu_B);
Nu_B_std = std(Nu_B);
% Average Nu from weighted Subchannel Nu
Av_Nu_B = Nu_S2B .* w2 + Nu_S5B .* w5 + Nu_S22B .* w22 + ...
    Nu_S26B .* w26 + Nu_S33B .* w33;
Av_Nu_B_av = mean(Av_Nu_B);
Av_Nu_B_std = std(Av_Nu_B);
% Average Nu KIT methodology
Tw_B_kit = (Tw_S2B ./ 4. + Tw_S5B ./4. + Tw_S22B ./ 4. + Tw_S26B ./6. + Tw_S33B ./12.);
HTC_B_kit = q_s ./ (Tw_B_kit - TbulkB);
Nu_B_kit = HTC_B_kit .* D_h ./ LBE_cond;
Nu_B_kit_av  = mean(Nu_B_kit);
Nu_B_kit_std = std(Nu_B_kit);
%-------------------------------%
%           SECTION C           %
%-------------------------------%
%----Re and Pr on the section C----%
% Tb_avC = (TC_FPS_e(:,11) + TC_FPS_e(:,12) + TC_FPS_e(:,13)+...
%     TC_FPS_e(:,14)+ TC_FPS_e(:,15))./5.;
[LBE_cp, LBE_cond, LBE_rho, LBE_mi] = LBE(TbulkC+273.15);
LBE_cp = LBE_cp + normrnd(0,7./100.*LBE_cp,n,1);
LBE_cond = LBE_cond + normrnd(0,5./100.*LBE_cond,n,1);
LBE_mi = LBE_mi + normrnd(0,5./100.*LBE_mi,n,1);
Re_C = Mf ./ Area .* D_h ./ LBE_mi;
Re_C_av = mean(Re_C);
Re_C_std = std(Re_C);
Pr_C = LBE_mi .* LBE_cp ./ LBE_cond;
Pr_C_av = mean(Pr_C);
Pr_C_std = std(Pr_C);
Pe_C = Re_C .* Pr_C;
Pe_C_av = mean(Pe_C);
Pe_C_std = std(Pe_C);
%---------- Subchannel S2 ---------%
Tw_S2C = (TC_FPS_w(:, 42) + TC_FPS_w(:, 44) + TC_FPS_w(:, 50))/3.;
Tw_S2C_av = mean(Tw_S2C);
Tw_S2C_std = std(Tw_S2C);
Tb_S2C = TC_FPS_e(:, 11);
Tb_S2C_av = mean(Tb_S2C);
Tb_S2C_std = std(Tb_S2C);
HTC_S2C = q_s ./ (Tw_S2C-Tb_S2C);
HTC_S2C_av = mean(HTC_S2C);
HTC_S2C_std = std(HTC_S2C);
[~, LBE_cond, ~, ~] = LBE(Tb_S2C+273.15); % vettori prop
LBE_cond = LBE_cond + normrnd(0,5./100.*LBE_cond,n,1);
Nu_S2C = HTC_S2C .* D_h ./ LBE_cond;
Nu_S2C_av = mean(Nu_S2C);
Nu_S2C_std = std(Nu_S2C);
%---------- Subchannel S5 ---------%
Tw_S5C = (TC_FPS_w(:, 43) + TC_FPS_w(:, 45) + TC_FPS_w(:, 46))./3.;
Tw_S5C_av = mean(Tw_S5C);
Tw_S5C_std = std(Tw_S5C);
Tb_S5C = TC_FPS_e(:, 12);
Tb_S5C_av = mean(Tb_S5C);
Tb_S5C_std = std(Tb_S5C);
HTC_S5C = q_s ./ (Tw_S5C-Tb_S5C);
HTC_S5C_av = mean(HTC_S5C);
HTC_S5C_std = std(HTC_S5C);
[~, LBE_cond, ~, ~] = LBE(Tb_S5C+273.15); % vettori prop
LBE_cond = LBE_cond + normrnd(0,5./100.*LBE_cond,n,1);
Nu_S5C = HTC_S5C .* D_h ./ LBE_cond;
Nu_S5C_av = mean(Nu_S5C);
Nu_S5C_std = std(Nu_S5C);
%---------- Subchannel S22 ---------%
Tw_S22C = (TC_FPS_w(:, 47) + TC_FPS_w(:, 49) + TC_FPS_w(:, 52))./3.;
Tw_S22C_av = mean(Tw_S22C);
Tw_S22C_std = std(Tw_S22C);
Tb_S22C = TC_FPS_e(:, 13);
Tb_S22C_av = mean(Tb_S22C);
Tb_S22C_std = std(Tb_S22C);
HTC_S22C = q_s ./ (Tw_S22C-Tb_S22C);
HTC_S22C_av = mean(HTC_S22C);
HTC_S22C_std = std(HTC_S22C);
```

```
[~, LBE_cond, ~, ~] = LBE(Tb_S22C+273.15); % vettori prop
LBE_cond = LBE_cond + normrnd(0,5./100.*LBE_cond,n,1);
Nu_S22C = HTC_S22C .* D_h ./ LBE_cond;
Nu_S22C_av = mean(Nu_S22C);
Nu_S22C_std = std(Nu_S22C);
%---------- Subchannel S26 ---------%
Tw_S26C = (TC_FPS_w(:, 53) + TC_FPS_w(:, 54))./2.;
Tw_S26C_av = mean(Tw_S26C);
Tw_S26C_std = std(Tw_S26C);
Tb_S26C = TC_FPS_e(:, 14);
Tb_S26C_av = mean(Tb_S26C);
Tb_S26C_std = std(Tb_S26C);
HTC_S26C = q_s ./ (Tw_S26C-Tb_S26C);
HTC_S26C_av = mean(HTC_S26C);
HTC_S26C_std = std(HTC_S26C);
[~, LBE_cond, ~, ~] = LBE(Tb_S26C+273.15); % vettori prop
LBE_cond = LBE_cond + normrnd(0,5./100.*LBE_cond,n,1);
Nu_S26C = HTC_S26C .* D_h ./ LBE_cond;
Nu_S26C_av = mean(Nu_S26C);
Nu_S26C_std = std(Nu_S26C);
%---------- Subchannel S33 ---------%
Tw_S33C = TC_FPS_w(:, 51);
Tw_S33C_av = mean(Tw_S33C);
Tw_S33C_std = std(Tw_S33C);
Tb_S33C = TC_FPS_e(:, 15);
Tb_S33C_av = mean(Tb_S33C);
Tb_S33C_std = std(Tb_S33C);
HTC_S33C = q_s ./ (Tw_S33C-Tb_S33C);
HTC_S33C_av = mean(HTC_S33C);
HTC_S33C_std = std(HTC_S33C);
[~, LBE_cond, ~, ~] = LBE(Tb_S33C+273.15); % vettori prop
LBE_cond = LBE_cond + normrnd(0,5./100.*LBE_cond,n,1);
Nu_S33C = HTC_S22C .* D_h ./ LBE_cond;
Nu_S33C_av = mean(Nu_S33C);
Nu_S33C_std = std(Nu_S33C);
%------------------------------%
%       Average Nu in section C     %
%------------------------------%
TwallC = Tw_S5C .* (w2+w5) + Tw_S22C .* w22+...
    Tw_S26C .* w26 + Tw_S33C .* w33;
TwallC_av = mean (TwallC);
TwallC_std = std(TwallC);
HTC_C = q_s ./ (TwallC - TbulkC);
HTC_C_av = mean(HTC_C);
HTC_C_std = std(HTC_C);
[~, LBE_cond, ~, ~] = LBE(TbulkC+273.15);
LBE_cond = LBE_cond + normrnd(0,5./100.*LBE_cond,n,1);
Nu_C = HTC_C .* D_h ./ LBE_cond;
Nu_C_av = mean(Nu_C);
Nu_C_std = std(Nu_C);
% Average Nu from weighted Subchannel Nu
Av_Nu_C = Nu_S5C .* (w5+w2) + Nu_S22C .* w22 + ...
    Nu_S26C .* w26 + Nu_S33C .* w33;
Av_Nu_C_av = mean(Av_Nu_C);
Av_Nu_C_std = std(Av_Nu_C);
% Average Nu KIT methodology
Tw_C_kit = (Tw_S2C ./ 4. + Tw_S5C ./ 4. + Tw_S22C ./4. + Tw_S26C ./6. + Tw_S33C ./12.);
HTC_C_kit = q_s ./ (Tw_C_kit - TbulkC);
Nu_C_kit = HTC_C_kit .* D_h ./ LBE_cond;
Nu_C_kit_av  = mean(Nu_C_kit);
Nu_C_kit_std = std(Nu_C_kit);
%------------------------------%
%         OUTPUT file          %
%------------------------------%
Av_values = [Q_av/0.97;
Mf_av;Tinlet_av;Toutlet_av;mean(P101);mean(P102);mean(P103);mean(P104);...
    mean(P105);mean(P110);mean(DP_FPS);mean(DP_head);mean(TP101);...
    mean(TP102);mean(TP103);mean(TP104);mean(TP105);mean(TP106);...

mean(TP107);mean(TFM101);TC_FPS_av;TC_FPS_w_av(:,16:67)';TbulkA_av;TwallA_av;Re_A_av;Pr_A_av;P
e_A_av;Nu_A_av;Nu_A_kit_av;...
    Nu_S2A_av;Nu_S5A_av;
Nu_S22A_av;Nu_S26A_av;Nu_S33A_av;Av_Nu_A_av;TbulkB_av;TwallB_av;Re_B_av;...
    Pr_B_av;Pe_B_av;Nu_B_av;Nu_B_kit_av;Nu_S2B_av;Nu_S5B_av;Nu_S22B_av;Nu_S26B_av;...
```

```
Nu_S33B_av;Av_Nu_B_av;TbulkC_av;TwallC_av;Re_C_av;Pr_C_av;Pe_C_av;Nu_C_av;Nu_C_kit_av;Nu_S2C_a
v;Nu_S5C_av;...
    Nu_S22C_av;Nu_S26C_av;Nu_S33C_av;Av_Nu_C_av];


Std_values = [Q_std; Mf_std;Tinlet_std;Toutlet_std;std(P101);std(P102);std(P103);std(P104);...
    std(P105);std(P110);std(DP_FPS);std(DP_head);std(TP101);...
    std(TP102);std(TP103);std(TP104);std(TP105);std(TP106);...

std(TP107);std(TFM101);TC_FPS_std;TC_FPS_w_std(:,16:67)';TbulkA_std;TwallA_std;Re_A_std;Pr_A_s
td;Pe_A_std;Nu_A_std;Nu_A_kit_std;...
    Nu_S2A_std;Nu_S5A_std;
Nu_S22A_std;Nu_S26A_std;Nu_S33A_std;Av_Nu_A_std;TbulkB_std;TwallB_std;Re_B_std;...
    Pr_B_std;Pe_B_std;Nu_B_std;Nu_B_kit_std;Nu_S2B_std;Nu_S5B_std;Nu_S22B_std;Nu_S26B_std;...
    Nu_S33B_std;Av_Nu_B_std;TbulkC_std;TwallC_std;Re_C_std;...
    Pr_C_std;Pe_C_std;Nu_C_std;Nu_C_kit_std;Nu_S2C_std;Nu_S5C_std;...
    Nu_S22C_std;Nu_S26C_std;Nu_S33C_std;Av_Nu_C_std];


fprintf(fileIDO, formatOh,'Case','Power','Mass Flow Rate','T in FPS','T out
FPS','P101','P102','P103','P104','P105','P110','DP_FPS','DP_head','TP101','TP102','TP103','TP1
04','TP105','TP106','TP107','TFM101',...

'TC_FPS_01','TC_FPS_02','TC_FPS_03','TC_FPS_04','TC_FPS_05','TC_FPS_06','TC_FPS_07','TC_FPS_08
','TC_FPS_09','TC_FPS_10','TC_FPS_11','TC_FPS_12','TC_FPS_13','TC_FPS_14','TC_FPS_15','TC_FPS_
16','TC_FPS_17','TC_FPS_18','TC_FPS_19','TC_FPS_20','TC_FPS_21','TC_FPS_22','TC_FPS_23','TC_FP
S_24','TC_FPS_25','TC_FPS_26','TC_FPS_27','TC_FPS_28','TC_FPS_29','TC_FPS_30','TC_FPS_31','TC_
FPS_32','TC_FPS_33','TC_FPS_34','TC_FPS_35','TC_FPS_36','TC_FPS_37','TC_FPS_38','TC_FPS_39','T
C_FPS_40','TC_FPS_41','TC_FPS_42','TC_FPS_43','TC_FPS_44','TC_FPS_45','TC_FPS_46','TC_FPS_47',
'TC_FPS_48','TC_FPS_49','TC_FPS_50','TC_FPS_51','TC_FPS_52','TC_FPS_53','TC_FPS_54','TC_FPS_55
','TC_FPS_56','TC_FPS_57','TC_FPS_58','TC_FPS_59','TC_FPS_60','TC_FPS_61','TC_FPS_62','TC_FPS_
63','TC_FPS_64','TC_FPS_65','TC_FPS_66','TC_FPS_67',...

'TC_FPS_w_16','TC_FPS_w_17','TC_FPS_w_18','TC_FPS_w_19','TC_FPS_w_20','TC_FPS_w_21','TC_FPS_w_
22','TC_FPS_w_23','TC_FPS_w_24','TC_FPS_w_25','TC_FPS_w_26','TC_FPS_w_27','TC_FPS_w_28','TC_FP
S_w_29','TC_FPS_w_30','TC_FPS_w_31','TC_FPS_w_32','TC_FPS_w_33','TC_FPS_w_34','TC_FPS_w_35','T
C_FPS_w_36','TC_FPS_w_37','TC_FPS_w_38','TC_FPS_w_39','TC_FPS_w_40','TC_FPS_w_41','TC_FPS_w_42
','TC_FPS_w_43','TC_FPS_w_44','TC_FPS_w_45','TC_FPS_w_46','TC_FPS_w_47','TC_FPS_w_48','TC_FPS_
w_49','TC_FPS_w_50','TC_FPS_w_51','TC_FPS_w_52','TC_FPS_w_53','TC_FPS_w_54','TC_FPS_w_55','TC_
FPS_w_56','TC_FPS_w_57','TC_FPS_w_58','TC_FPS_w_59','TC_FPS_w_60','TC_FPS_w_61','TC_FPS_w_62',
'TC_FPS_w_63','TC_FPS_w_64','TC_FPS_w_65','TC_FPS_w_66','TC_FPS_w_67',...

'Tbulk_A','Twall_A','Re_A','Pr_A','Pe_A','Nu1_A','Nu_A_kit','Nu_S2_A','Nu_S5_A','Nu_S22_A','Nu
_S26_A','Nu_S33_A','Nu2_A',...

'Tbulk_B','Twall_B','Re_B','Pr_B','Pe_B','Nu1_B','Nu_B_kit','Nu_S2_B','Nu_S5_B','Nu_S22_B','Nu
_S26_B','Nu_S33_B','Nu2_B',...

'Tbulk_C','Twall_C','Re_C','Pr_C','Pe_C','Nu1_C','Nu_C_kit','Nu_S2_C','Nu_S5_C','Nu_S22_C','Nu
_S26_C','Nu_S33_C','Nu2_C',...
    'Power_std','Mass Flow Rate_std','T in FPS_std','T out
FPS_std','P101_std','P102_std','P103_std','P104_std','P105_std','P110_std','DP_FPS_std','DP_he
ad_std','TP101_std','TP102_std','TP103_std','TP104_std','TP105_std','TP106_std','TP107_std','T
FM101_std',...

'TC_FPS_01_std','TC_FPS_02_std','TC_FPS_03_std','TC_FPS_04_std','TC_FPS_05_std','TC_FPS_06_std
','TC_FPS_07_std','TC_FPS_08_std','TC_FPS_09_std','TC_FPS_10_std',
'TC_FPS_11_std','TC_FPS_12_std','TC_FPS_13_std','TC_FPS_14_std','TC_FPS_15_std','TC_FPS_16_std
','TC_FPS_17_std','TC_FPS_18_std','TC_FPS_19_std','TC_FPS_20_std','TC_FPS_21_std','TC_FPS_22_s
td','TC_FPS_23_std','TC_FPS_24_std','TC_FPS_25_std','TC_FPS_26_std','TC_FPS_27_std','TC_FPS_28
_std','TC_FPS_29_std','TC_FPS_30_std','TC_FPS_31_std','TC_FPS_32_std','TC_FPS_33_std','TC_FPS_
34_std','TC_FPS_35_std','TC_FPS_36_std','TC_FPS_37_std','TC_FPS_38_std','TC_FPS_39_std','TC_FP
S_40_std','TC_FPS_41_std','TC_FPS_42_std','TC_FPS_43_std','TC_FPS_44_std','TC_FPS_45_std','TC_
FPS_46_std','TC_FPS_47_std','TC_FPS_48_std','TC_FPS_49_std','TC_FPS_50_std','TC_FPS_51_std','T
C_FPS_52_std','TC_FPS_53_std','TC_FPS_54_std','TC_FPS_55_std','TC_FPS_56_std','TC_FPS_57_std',
'TC_FPS_58_std','TC_FPS_59_std','TC_FPS_60_std','TC_FPS_61_std','TC_FPS_62_std','TC_FPS_63_std
','TC_FPS_64_std','TC_FPS_65_std','TC_FPS_66_std','TC_FPS_67_std',...

'TC_FPSw_16_std','TC_FPSw_17_std','TC_FPSw_18_std','TC_FPSw_19_std','TC_FPSw_20_std','TC_FPSw_
21_std','TC_FPSw_22_std','TC_FPSw_23_std','TC_FPSw_24_std','TC_FPSw_25_std','TC_FPSw_26_std','
TC_FPSw_27_std','TC_FPSw_28_std','TC_FPSw_29_std','TC_FPSw_30_std','TC_FPSw_31_std','TC_FPSw_3
2_std','TC_FPSw_33_std','TC_FPSw_34_std','TC_FPSw_35_std','TC_FPSw_36_std','TC_FPSw_37_std','T
C_FPSw_38_std','TC_FPSw_39_std','TC_FPSw_40_std','TC_FPSw_41_std','TC_FPSw_42_std','TC_FPSw_43
_std','TC_FPSw_44_std','TC_FPSw_45_std','TC_FPSw_46_std','TC_FPSw_47_std','TC_FPSw_48_std','TC
_FPSw_49_std','TC_FPSw_50_std','TC_FPSw_51_std','TC_FPSw_52_std','TC_FPSw_53_std','TC_FPSw_54_
```

```
std','TC_FPSw_55_std','TC_FPSw_56_std','TC_FPSw_57_std','TC_FPSw_58_std','TC_FPSw_59_std','TC_
FPSw_60_std','TC_FPSw_61_std','TC_FPSw_62_std','TC_FPSw_63_std','TC_FPSw_64_std','TC_FPSw_65_s
td','TC_FPSw_66_std','TC_FPSw_67_std',...

'Tbulk_A_std','Twall_A_std','Re_A_std','Pr_A_std','Pe_A_std','Nu1_A_std','Nu_A_kit_std','Nu_S2
_A_std','Nu_S5_A_std','Nu_S22_A_std','Nu_S26_A_std','Nu_S33_A_std','Nu2_A_std',...

'Tbulk_B_std','Twall_B_std','Re_B_std','Pr_B_std','Pe_B_std','Nu1_B_std','Nu_B_kit_std','Nu_S2
_B_std','Nu_S5_B_std','Nu_S22_B_std','Nu_S26_B_std','Nu_S33_B_std','Nu2_B_std',...

'Tbulk_C_std','Twall_C_std','Re_C_std','Pr_C_std','Pe_C_std','Nu1_C_std','Nu_C_kit_std','Nu_S2
_C_std','Nu_S5_C_std','Nu_S22_C_std','Nu_S26_C_std','Nu_S33_C_std','Nu2_C_std');
fprintf(fileIDO, '%s \n', '');
fprintf(fileIDO, '%s \t', 'P269');
fprintf(fileIDO, formatO, Av_values);

fprintf(fileIDO, formatO, Std_values);
fprintf(fileIDO, '%s \n', '');
```

- **Annex B**

Case	Power [kW]	mfr NACIE [kg/s]	mfr MYRRHA [kg/s]	T in FPS	T out FPS	Pe_A	Nu1_A	Nu2_A
P103	11.02	0.36	2.08	190.10	393.80	30.00	6.28	7.61
P102b	10.95	0.68	3.91	187.10	294.70	57.10	6.79	7.85
P102	10.95	0.72	4.12	186.80	288.10	60.24	6.87	7.88
P204	20.01	0.73	4.21	191.30	374.30	60.74	6.02	6.88
P11X0	10.96	1.06	6.11	185.60	253.90	89.68	7.54	8.42
P214	36.00	1.15	6.65	229.50	439.50	90.71	6.43	7.00
P28X0	28.01	1.17	6.73	215.20	374.60	94.23	6.82	7.53
P20X0	19.96	1.50	8.62	189.30	277.80	125.80	6.96	8.13
P43X0	43.01	1.63	9.38	226.20	403.10	128.90	6.76	7.31
P213	36.00	2.23	12.82	233.50	341.30	175.40	7.34	7.96
P224	52.00	2.24	12.89	243.60	400.10	173.70	7.82	8.31
P100	10.97	2.28	13.13	182.40	214.20	194.60	8.73	10.12
P218	43.00	2.80	16.14	240.00	342.30	218.50	7.87	8.39
P099	11.00	2.92	16.80	192.20	217.20	245.90	11.00	11.57
P203	20.04	3.11	17.93	203.20	245.70	257.40	8.74	9.93
P217	43.00	3.21	18.51	245.90	335.30	249.30	8.17	8.66
P265	53.99	3.23	18.58	242.80	354.60	250.90	8.18	8.61
P212	35.99	3.33	19.20	241.50	313.20	259.50	8.03	8.64
P223	52.00	3.40	19.58	250.00	352.50	263.10	8.65	9.13
P269	108.00	3.95	22.76	264.90	448.50	297.30	8.29	8.77
P202	19.96	4.17	24.02	202.50	234.10	347.40	10.17	11.25

Case	Power [kW]	mfr NACIE [kg/s]	mfr MYRRHA [kg/s]	T in FPS	T out FPS	Pe_B	Nu1_B	Nu2_B
P103	11.02	0.36	2.08	190.10	393.80	26.56	5.52	6.31
P102b	10.95	0.68	3.91	187.10	294.70	53.47	5.63	6.28
P102	10.95	0.72	4.12	186.80	288.10	56.85	5.63	7.10
P204	20.01	0.73	4.21	191.30	374.30	54.64	5.61	6.84
P11X0	10.96	1.06	6.11	185.60	253.90	86.27	5.87	7.36
P214	36.00	1.15	6.65	229.50	439.50	80.73	5.32	6.65
P28X0	28.01	1.17	6.73	215.20	374.60	85.32	5.76	7.51
P20X0	19.96	1.50	8.62	189.30	277.80	118.50	6.32	7.59
P43X0	43.01	1.63	9.38	226.20	403.10	116.60	6.20	7.39
P213	36.00	2.23	12.82	233.50	341.30	165.30	6.21	7.40
P224	52.00	2.24	12.89	243.60	400.10	159.90	5.97	6.89
P100	10.97	2.28	13.13	182.40	214.20	191.10	6.62	8.13
P218	43.00	2.80	16.14	240.00	342.30	206.60	7.29	8.12
P099	11.00	2.92	16.80	192.20	217.20	241.30	8.13	9.08
P203	20.04	3.11	17.93	203.20	245.70	251.40	7.98	8.73
P217	43.00	3.21	18.51	245.90	335.30	237.20	7.32	7.99
P265	53.99	3.23	18.58	242.80	354.60	235.20	7.22	7.96
P212	35.99	3.33	19.20	241.50	313.20	250.90	7.06	7.85
P223	52.00	3.40	19.58	250.00	352.50	247.30	7.81	8.24
P269	108.00	3.95	22.76	264.90	448.50	269.60	7.18	7.82
P202	19.96	4.17	24.02	202.50	234.10	338.40	8.82	9.37

Case	Power [kW]	mfr NACIE [kg/s]	mfr MYRRHA [kg/s]	T in FPS	T out FPS	Pe_C	Nu1_C	Nu2_C
P103	11.02	0.36	2.08	190.10	393.80	23.90	5.86	6.95
P102b	10.95	0.68	3.91	187.10	294.70	50.31	6.29	8.64
P102	10.95	0.72	4.12	186.80	288.10	53.47	6.18	8.60
P204	20.01	0.73	4.21	191.30	374.30	49.53	4.83	7.20
P11X0	10.96	1.06	6.11	185.60	253.90	82.75	6.41	10.31
P214	36.00	1.15	6.65	229.50	439.50	72.64	4.67	7.79
P28X0	28.01	1.17	6.73	215.20	374.60	79.07	5.10	8.51
P20X0	19.96	1.50	8.62	189.30	277.80	112.60	5.05	8.30
P43X0	43.01	1.63	9.38	226.20	403.10	106.30	5.00	8.22
P213	36.00	2.23	12.82	233.50	341.30	155.40	7.20	9.13
P224	52.00	2.24	12.89	243.60	400.10	146.40	5.25	9.04
P100	10.97	2.28	13.13	182.40	214.20	186.80	5.91	9.66
P218	43.00	2.80	16.14	240.00	342.30	196.10	6.10	9.44
P099	11.00	2.92	16.80	192.20	217.20	237.60	8.65	11.80
P203	20.04	3.11	17.93	203.20	245.70	243.50	6.43	9.61
P217	43.00	3.21	18.51	245.90	335.30	225.70	9.12	9.76
P265	53.99	3.23	18.58	242.80	354.60	222.40	6.35	9.47
P212	35.99	3.33	19.20	241.50	313.20	241.60	9.41	10.01
P223	52.00	3.40	19.58	250.00	352.50	234.50	6.07	9.97
P269	108.00	3.95	22.76	264.90	448.50	245.90	6.95	9.64
P202	19.96	4.17	24.02	202.50	234.10	333.20	7.08	10.11

Case	Power [kW]	mfr NACIE [kg/s]	mfr MYRRHA [kg/s]	Nu_S2_A	Nu_S5_A	Nu_S22_A	Nu_S26_A	Nu_S33_A
P103	11.02	0.36	2.08	7.36	4.99	11.75	3.53	6.11
P102b	10.95	0.68	3.91	7.49	5.45	11.55	4.02	6.65
P102	10.95	0.72	4.12	7.49	5.45	11.50	4.15	6.72
P204	20.01	0.73	4.21	7.92	5.17	10.03	3.78	5.49
P11X0	10.96	1.06	6.11	7.83	5.89	11.89	4.83	7.38
P214	36.00	1.15	6.65	8.00	5.52	9.54	4.44	5.90
P28X0	28.01	1.17	6.73	8.33	5.60	10.30	4.40	6.59
P20X0	19.96	1.50	8.62	8.95	5.97	12.62	5.41	5.37
P43X0	43.01	1.63	9.38	8.44	6.02	9.99	4.96	5.94
P213	36.00	2.23	12.82	9.08	6.65	10.98	5.88	6.10
P224	52.00	2.24	12.89	13.20	9.81	9.80	5.56	7.21
P100	10.97	2.28	13.13	10.23	7.16	15.59	7.55	6.60
P218	43.00	2.80	16.14	9.71	7.09	11.13	7.34	6.26
P099	11.00	2.92	16.80	10.40	8.21	14.68	8.73	10.73
P203	20.04	3.11	17.93	10.81	7.60	14.73	8.08	6.46
P217	43.00	3.21	18.51	10.34	7.42	11.41	6.59	6.97
P265	53.99	3.23	18.58	10.35	7.40	11.06	7.76	6.60
P212	35.99	3.33	19.20	10.15	7.47	11.82	6.60	6.55
P223	52.00	3.40	19.58	13.86	10.62	10.83	6.44	7.83
P269	108.00	3.95	22.76	10.48	7.71	11.14	8.62	6.44
P202	19.96	4.17	24.02	11.56	8.43	15.89	10.51	7.55

Case	Power [kW]	mfr NACIE [kg/s]	mfr MYRRHA [kg/s]	Nu_S2_B	Nu_S5_B	Nu_S22_B	Nu_S26_B	N
P103	11.02	0.36	2.08	10.27	7.65	8.14	3.11	5.
P102b	10.95	0.68	3.91	10.47	9.80	9.90	2.90	3.
P102	10.95	0.72	4.12	10.50	9.97	10.30	2.89	5.
P204	20.01	0.73	4.21	11.88	8.64	9.49	3.07	5.
P11X0	10.96	1.06	6.11	11.00	10.52	10.55	3.06	5.
P214	36.00	1.15	6.65	9.04	9.18	10.16	3.46	4.
P28X0	28.01	1.17	6.73	9.75	10.46	11.82	3.38	4.
P20X0	19.96	1.50	8.62	13.54	9.45	10.28	3.49	5.
P43X0	43.01	1.63	9.38	13.04	9.29	9.96	3.50	5.
P213	36.00	2.23	12.82	9.94	9.92	10.86	4.24	4.
P224	52.00	2.24	12.89	9.65	9.99	9.59	4.58	4.
P100	10.97	2.28	13.13	11.82	11.01	12.14	4.88	4.
P218	43.00	2.80	16.14	10.71	9.80	10.76	4.56	6.
P099	11.00	2.92	16.80	12.04	11.33	11.73	4.77	7.
P203	20.04	3.11	17.93	13.18	10.40	10.88	5.05	7.
P217	43.00	3.21	18.51	9.99	10.29	10.60	5.52	6.
P265	53.99	3.23	18.58	10.73	10.08	10.47	5.09	6.
P212	35.99	3.33	19.20	10.01	10.33	10.67	5.05	5.
P223	52.00	3.40	19.58	9.35	10.39	10.19	5.77	7.
P269	108.00	3.95	22.76	10.40	9.99	10.07	5.65	5.
P202	19.96	4.17	24.02	13.31	11.02	11.15	5.95	8.

Case	Power [kW]	mfr NACIE [kg/s]	mfr MYRRHA [kg/s]	Nu_S5_C	Nu_S22_C	Nu_S26_C	Nu_S33_C
P103	11.02	0.36	2.08	6.69	7.87	3.55	7.85
P102b	10.95	0.68	3.91	8.11	10.05	3.29	10.12
P102	10.95	0.72	4.12	8.32	9.98	3.24	10.03
P204	20.01	0.73	4.21	7.09	8.22	3.14	8.29
P11X0	10.96	1.06	6.11	8.46	12.43	3.10	12.47
P214	36.00	1.15	6.65	7.53	8.88	3.22	9.12
P28X0	28.01	1.17	6.73	8.03	9.70	3.67	9.92
P20X0	19.96	1.50	8.62	7.97	9.45	3.61	9.64
P43X0	43.01	1.63	9.38	7.90	9.31	3.50	9.62
P213	36.00	2.23	12.82	9.20	10.24	4.21	10.48
P224	52.00	2.24	12.89	9.12	10.14	3.88	10.52
P100	10.97	2.28	13.13	9.32	10.94	4.58	11.05
P218	43.00	2.80	16.14	8.85	10.59	4.62	10.92
P099	11.00	2.92	16.80	10.44	13.79	4.64	13.89
P203	20.04	3.11	17.93	9.54	10.57	5.47	10.76
P217	43.00	3.21	18.51	10.00	10.72	5.30	10.97
P265	53.99	3.23	18.58	9.40	10.45	4.81	10.87
P212	35.99	3.33	19.20	10.39	10.94	5.61	11.19
P223	52.00	3.40	19.58	10.05	10.97	5.15	11.37
P269	108.00	3.95	22.76	11.90	10.09	5.31	10.65
P202	19.96	4.17	24.02	9.97	10.93	6.65	11.09